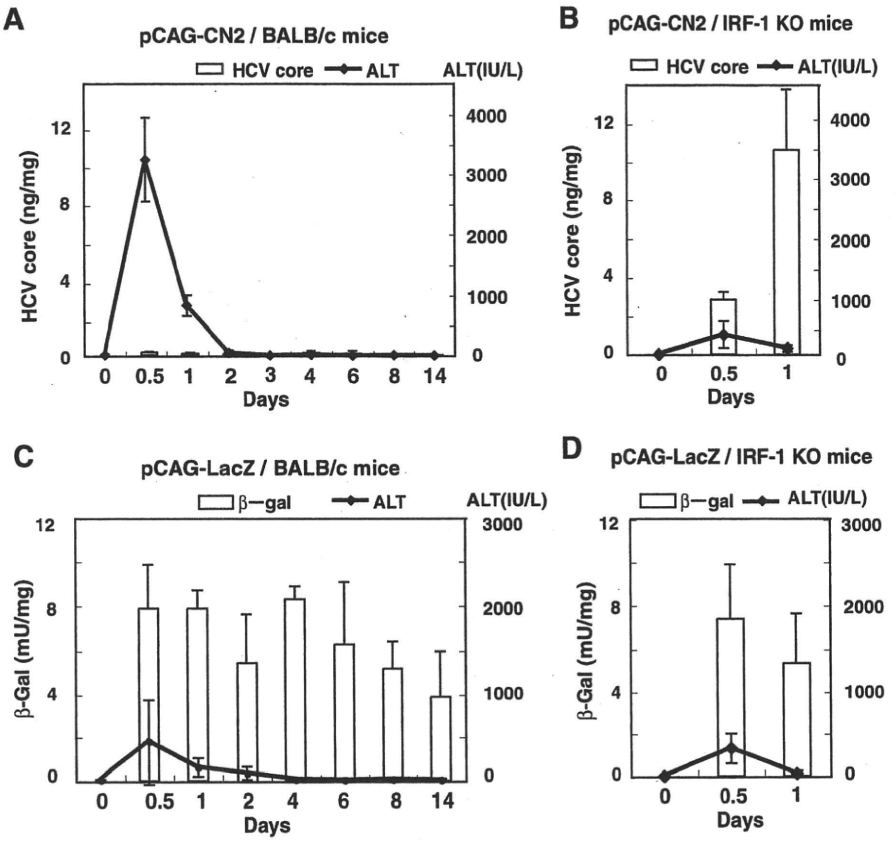

Fig. 4. Quantification of HCV core protein production and serum ALT levels in wild-type BALB/c mice and IRF-1 knockout BALB/c mice hydrodynamically transfected with expression plasmids. **A**: Results for wild-type BALB/c mice injected with pCAG-CN2 (Fse). HCV core protein in the liver was barely detectable at day 0.5 (0.123 ± 0.045 ng/mg) and declined gradually thereafter. The serum ALT level peaked on day 0.5 ($3{,}256 \pm 703$ IU/L) and declined gradually thereafter. **B**: Results for IRF-1 knock out BALB/c mice injected with pCAG-CN2 (Fse). HCV core protein levels in the hepatocytes was most strongly detected on days 0.5 (2.9 ± 0.4 ng/mg) and 1 (10.7 ± 3.1 ng/mg). Serum ALT was suppressed on day 0.5 (295 ± 197 IU/L). **C**: Results for BALB/c mice injected with pCAG-LacZ. Liver β-gal levels were first detectable on day 0.5 (7.9 ± 2.0 mU/mg) and were consistently detectable until day 14 (3.9 ± 2.1 mU/mg). The serum ALT level (450 ± 490 IU/L) was lower than that shown in Figure 2A ($3{,}256 \pm 703$ IU/L) at day 0.5, and returned to the baseline level after day 2. **D**: Results from IRF-1 knockout BALB/c mice injected with pCAG-LacZ. Liver β-gal levels were detected on days 0.5 (7.4 ± 2.5 mU) and 1 (5.4 ± 2.3 mU). The serum ALT level was (352 ± 178 IU/L) on day 0.5.

serum IFN-γ was not detected after transfection with pEF-core expression plasmids in CN2-8 IRF-1 (Fig. 5C). Serum IFN-γ secretion was suppressed in NK cell-depleted CN2-29 Tg mice and was not stimulated by pCAL-LacZ plasmid injection (Fig. 5D,E).

DISCUSSION

Immune responses to HCV during the acute phase of infection might play a crucial role in determining whether HCV is eliminated or is able to persist in the body. However, acute HCV infection is rarely symptomatic, making it tremendously difficult to analyze in vivo. In the present study, we generated an acute HCV model for the first time by using Tg mice with conditional expression regulated by the Cre/*loxP* system. Because there were no viral vector effects, we were able to observe HCV-specific innate immunity by using hydrodynamic transfection techniques.

NK cells constitute the first line of host defense against invading pathogens. Activated NK cells play an essential role in recruiting virus-specific T cells and inducing antiviral immunity in the liver [French et al., 2003]. They also eliminate virus-infected hepatocytes directly by cytolytic mechanisms and indirectly by secreting cytokines, which induce an antiviral state in host cells. In vitro studies revealed that NK cells are activated by cytokines during acute HCV infection [Yoon et al., 2008] and play an important antiviral role by eliminating the virus, both by killing it directly and by producing cytokines such as IFN-γ [Golden-Mason and Rosen, 2006].

In the present study, hepatocyte necrosis and intrahepatic mononuclear cell infiltration were observed on days 0.5 and 1 in wild-type mice. These were associated with elevated levels of serum ALT and IFN-γ and with reduced levels of HCV core protein expression. In contrast, NK cell depletion by IRF-1 knockout or treatment with anti-IL-2 receptor-β antibody was

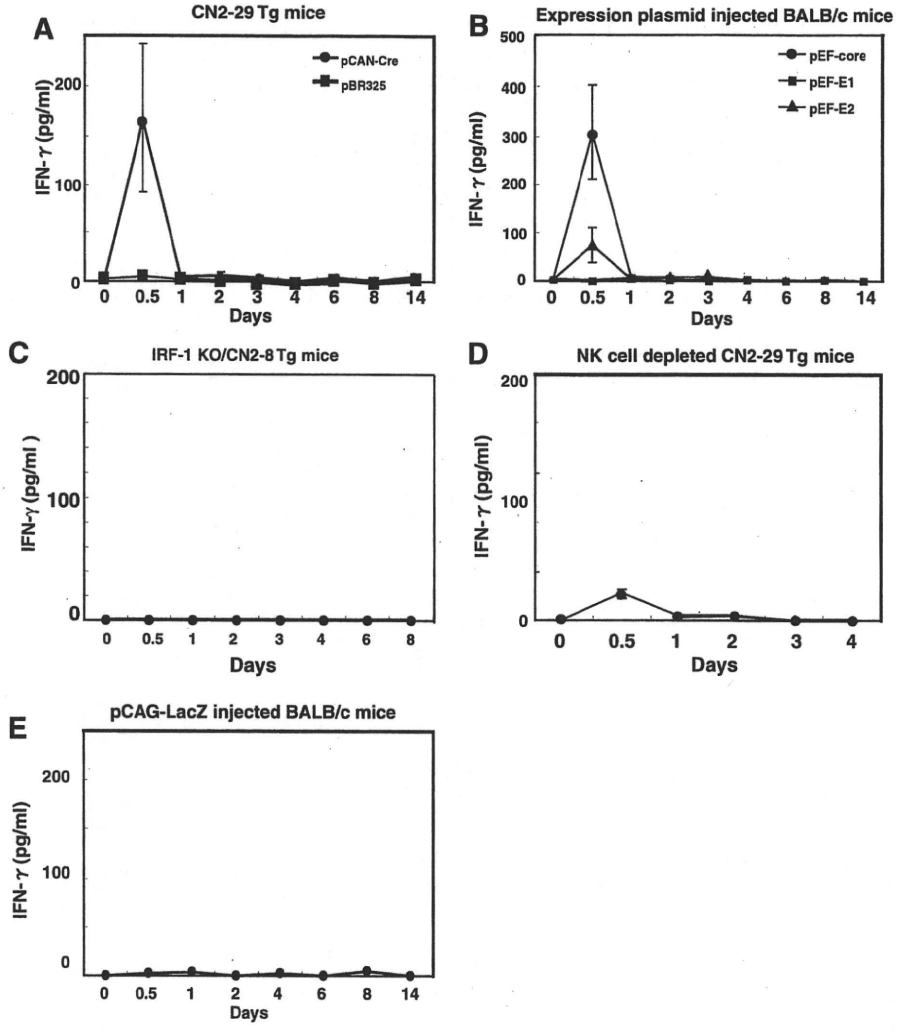

Fig. 5. Serum IFN-γ levels. **A**: Serum IFN-γ levels in CN2-29 Tg mice injected with the pCAN-Cre plasmid. Serum IFN-γ (168 ± 62 pg/ml) was detectable on day 0.5 in the pCAN-Cre plasmid-injected CN2-29 Tg mice (circle), but was not detectable in the pBR325 plasmid-injected CN2-29 Tg mice (square). **B**: Serum IFN-γ levels in mice injected with pEF-core (circle), -E1 (square), and -E2 (triangle) plasmids. **C**: Serum IFN-γ levels in IRF-1 knockout CN2-8 Tg mice injected with the pCAN-Cre plasmid. **D**: Serum IFN-γ levels in NK cell-depleted CN2-29 Tg mice injected with the pCAN-Cre plasmid. **E**: Serum IFN-γ levels in BALB/c mice injected with the pCAL-LacZ plasmid.

accompanied by increases in HCV core protein expression and decreased levels of ALT and IFN-γ on days 0.5 and 1. These results were confirmed by our histological observations. Cumulatively, these data suggest that the activity of NK cells might be directly cytolytic; specifically, they appear to play a significant role in IFN-γ secretion and elimination of virus-infected hepatocytes—especially core protein-presented hepatocytes—during the early phase of infection (days 0–1). Since the number of CD8+ cytotoxic T cells is greatly reduced in CN2-8 IRF-1 knockout mice, T cells usually participate in innate immunity, rather than acquired immunity. It has previously been reported that NK cells are required to recruit virus-specific T cells in response to HCV infection [Ahmad and Alvarez, 2004; Irshad et al., 2008]. These reports, together with our current work, indicate that NK cells play a very important antiviral role during acute HCV infection.

According to the results of the Southern and Northern blot analyses, non-cytolytic HCV core protein elimination takes place from days 3 to 14. However, this does not appear to be associated with IFN-γ or CD8+ cytotoxic T cells. Thus, during this period, another immune factor might be involved in eliminating HCV core protein in the hepatocytes without elevating ALT activity.

It is interesting that HCV core protein, but not E1 or E2 protein, induced the elevation of IFN-γ. Since HCV core protein is reported to activate NF-kB, thereby inducing the cellular inflammatory response [Dolganiuc et al., 2004], there is a possibility that HCV core protein

itself participates in the elevation of IFN-γ. IFN-γ is known to be expressed in the liver when infections spontaneously clear [Major et al., 2002; Thimme et al., 2002] and to be involved in the non-cytolytic control of HCV-infected hepatocytes [Thimme et al., 2001]. Additionally, IFN-γ inhibits the replication of subgenomic HCV replicons [Lohmann et al., 1999; Blight et al., 2000] in tissue culture cells [Frese et al., 2002; Lanford et al., 2003]. Since NK cells produce a large amount of IFN-γ when they are activated in response to inflammation, such as that caused by acute viral infection, both NK cells and IFN-γ may contribute to the innate immune response during acute HCV infection.

In conclusion, this Tg mouse model permits analysis of the HCV-specific immune response while avoiding adenovirus which has been applied for the study of HCV immunity. By using this model, we could determine some of the potential roles of NK cells in response to the presence of HCV structural protein during the early naïve phase of HCV infection. These findings confirm that NK cell activity is crucial in eliminating HCV-infected hepatocytes. This suggests that a potential new therapeutic approach is activation of NK cells in order to restore the innate immune defenses that control HCV replication.

ACKNOWLEDGMENTS

The authors wish to express their gratitude to Izumu Saito for his kind gift of the pCAN-Cre plasmid. We thank Dr. Masahiro Shuda for helpful comments during the preparation of this manuscript. We also thank Mitsugu Takahashi for breeding the transgenic mice.

REFERENCES

Ahmad A, Alvarez F. 2004. Role of NK and NKT cells in the immunopathogenesis of HCV-induced hepatitis. J Leukoc Biol 76:743–759.

Bigger CB, Brasky KM, Lanford RE. 2001. DNA microarray analysis of chimpanzee liver during acute resolving hepatitis C virus infection. J Virol 75:7059–7066.

Blight KJ, Kolykhalov AA, Rice CM. 2000. Efficient initiation of HCV RNA replication in cell culture. Science 290:1972–1974.

Carroll JM, Crompton T, Seery JP, Watt FM. 1997. Transgenic mice expressing IFN-gamma in the epidermis have eczema, hair hypopigmentation, and hair loss. J Invest Dermatol 108:412–422.

Crotta S, Stilla A, Wack A, D'Andrea A, Nuti S, D'Oro U, Mosca M, Filliponi F, Brunetto RM, Bonino F, Abrignani S, Valiante NM. 2002. Inhibition of natural killer cells through engagement of CD81 by the major hepatitis C virus envelope protein. J Exp Med 195:35–41.

Disson O, Haouzi D, Desagher S, Loesch K, Hahne M, Kremer EJ, Jacquet C, Lemon SM, Hibner U, Lerat H. Impaired clearance of virus-infected hepatocytes in transgenic mice expressing the hepatitis C virus polyprotein. Gastroenterology 2004. 126:859–872.

Dolganiuc A, Oak S, Kodys K, Golenbock DT, Finberg RW, Kurt-Jones E, Szabo G. 2004. Hepatitis C core and nonstructural 3 proteins trigger toll-like receptor 2-mediated pathways and inflammatory activation. Gastroenterology 127:1513–1524.

Duncan GS, Mittrucker HW, Kagi D, Matsuyama T, Mak TW. 1996. The transcription factor interferon regulatory factor-1 is essential for natural killer cell function *in vivo*. J Exp Med 184:2043–2048.

Ebihara T, Shingai M, Matsumoto M, Wakita T, Seya T. 2008. Hepatitis C virus-infected hepatocytes extrinsically modulate dendritic cell maturation to activate T cells and natural killer cells. Hepatology 48:48–58.

French AR, Yokoyama WM. 2003. Natural killer cells and viral infections. Curr Opin Immunol 15:45–51.

Frese M, Schwarzle V, Barth K, Krieger N, Lohmann V, Mihm S, Haller O, Bartenschlager R. 2002. Interferon-gamma inhibits replication of subgenomic and genomic hepatitis C virus RNAs. Hepatology 35:694–703.

Gerlach JT, Diepolder HM, Zachoval R, Gruener NH, Jung MC, Ulsenheimer A, Schraut WW, Schrirren CA, Waechtler M, Backmund M, Pape GR. 2003. Acute hepatitis C: High rate of both spontaneous and treatment-induced viral clearance. Gastroenterology 125:80–88.

Golden-Mason L, Madrigal-Estebas L, McGrath E, Conroy MJ, Ryan EJ, Hegarty JE, O'Farrelly C, Doherty DG. 2008. Altered natural killer cell subset distributions in resolved and persistent hepatitis C virus infection following single source exposure. Gut 57:1121–1128.

Golden-Mason L, Rosen HR. 2006. Natural killer cells: Primary target for hepatitis C virus immune evasion strategies? Liver Transpl 12:363–372.

Irshad M, Khushboo I, Singh S, Singh S. 2008. Hepatitis C virus (HCV): A review of immunological aspects. Int Rev Immunol 27:497–517.

Kashiwakuma T, Hasegawa A, Kajita T, Takata A, Mori H, Ohta Y, Tanaka E, Kiyosawa K, Tanaka T, Tanaka S, Hattori N, Kohara M. 1996. Detection of hepatitis C virus specific core protein in serum of patients by a sensitive fluorescence enzyme immunoassay (FEIA). J Immunol Methods 190:79–89.

Knapp S, Warshow U, Hegazy D, Brackbury L, Guha IN, Fowell A, Little AM, Alexander GJ, Rosenberg WM, Cramp ME, Khakoo SI. 2009. Consistent beneficial effects of killer cell immunoglobulin-like receptor 2DL3 and group 1 human leukocyte antigen-C following exposure to hepatitis C virus. Hepatology 51:1–8.

Lanford RE, Guerra B, Lee H, Averett DR, Pfeiffer B, Chavez D, Notvall L, Bigger C. 2003. Antiviral effect and virus-host interactions in response to alpha interferon, gamma interferon, poly(i)-poly(c), tumor necrosis factor alpha, and ribavirin in hepatitis C virus subgenomic replicons. J Virol 77:1092–1104.

Liu F, Song Y, Liu D. 1999. Hydrodynamics-based transfection in animals by systemic administration of plasmid DNA. Gene Ther 6:1258–1266.

Lohmann V, Korner F, Koch J, Herian U, Theilmann L, Bartenschlager R. 1999. Replication of subgenomic hepatitis C virus RNAs in a hepatoma cell line. Science 285:110–113.

Machida K, Tsukiyama-Kohara K, Seike E, Tone S, Shibasaki F, Shimizu M, Takahashi H, Funata N, Taya C, Yonekawa H, Kohara M. 2001. Inhibition of cytochrome c release in Fas-mediated signaling pathway in transgenic mice induced to express hepatitis C viral proteins. J Biol Chem 276:12140–12146.

Major ME, Mihalik K, Puig M, Rehermann B, Nascimbeni M, Rice CM, Feinstone SM. 2002. Previously infected and recovered chimpanzees exhibit rapid responses that control hepatitis C virus replication upon rechallenge. J Virol 76:6586–6595.

Matsuyama T, Kimura T, Kitagawa M, Pfeffer K, Kawakami T, Watanabe N, Kundig TM, Amakawa R, Kishihara K, Wakeham A. 1993. Targeted disruption of IRF-1 or IRF-2 results in abnormal type I IFN gene induction and aberrant lymphocyte development. Cell 75:83–97.

Minakuchi Y, Takeshita F, Kosaka N, Sasaki H, Yamamoto Y, Kouno M, Honma K, Nagahara S, Hanai K, Sano A, Kato T, Terada M, Ochiya T. 2004. Atelocollagen-mediated synthetic small interfering RNA delivery for effective gene silencing *in vitro* and *in vivo*. Nucleic Acids Res 32:e109.

Ochiya T, Nagahara S, Sano A, Itoh H, Terada M. 2001. Biomaterials for gene delivery: Atelocollagen-mediated controlled release of molecular medicines. Curr Gene Ther 1:31–52.

Ohteki T, Yoshida H, Matsuyama T, Duncan GS, Mak TW, Ohashi PS. 1998. The transcription factor interferon regulatory factor 1 (IRF-1) is important during the maturation of natural killer 1.1+ T cell receptor-alpha/beta+ (NK1+ T) cells, natural killer cells, and intestinal intraepithelial T cells. J Exp Med 187:967–972.

Su AI, Pezacki JP, Wodicka L, Brideau AD, Supekova L, Thimme R, Wieland S, Jens B, Purcell RH, Schultz PG, Chisari FV. 2002. Genomic analysis of the host response to hepatitis C virus infection. Proc Natl Acad Sci USA 99:15669–15674.

Takaku S, Nakagawa Y, Shimizu M, Norose Y, Maruyama I, Wakita T, Takano T, Kohara M, Takahashi H. 2003. Induction of hepatic injury by hepatitis C virus-specific CD8+ murine cytotoxic T

lymphocytes in transgenic mice expressing the viral structural genes. Biochem Biophys Res Commun 301:330–337.

Tanaka T, Kitamura F, Nagasaka Y, Kuida K, Suwa H, Miyasaka M. 1993. Selective long-term elimination of natural killer cells *in vivo* by an anti-interleukin 2 receptor beta chain monoclonal antibody in mice. J Exp Med 178:1103–1107.

Thimme R, Oldach D, Chang KM, Steiger C, Ray SC, Chisari FV. 2001. Determinants of viral clearance and persistence during acute hepatitis C virus infection. J Exp Med 194:1395–1406.

Thimme R, Bukh J, Spangenberg HC, Wieland S, Pemberton J, Steiger C, Govindarajan S, Purcell RH, Chisari FV. 2002. Viral and immunological determinants of hepatitis C virus clearance, persistence, and disease. Proc Natl Acad Sci USA 99:15661–15668.

Tseng CT, Klimpel GR. 2002. Binding of the hepatitis C virus envelope protein E2 to CD81 inhibits natural killer cell functions. J Exp Med 195:43–49.

Tsukiyama-Kohara K, Tone S, Maruyama I, Inoue K, Katsume A, Nuriya H, Ohmori H, Ohkawa J, Taira K, Hoshikawa Y, Shibasaki F, Reth M, Minatogawa Y, Kohara M. 2004. Activation of the CKI-CDK-Rb-E2F pathway in full genome hepatitis C virus-expressing cells. J Biol Chem 279:14531–14541.

Vidal-Castineira JR, Lopez ZA, Diaz PR, Alonso AR, Martinez BJ, Perez R, Fernandez SJ, Melon S, Prieto J, Rodrigo L, López LC. 2010. Effect of killer immunogloblin-like receptors in the response to combined treatment in patients with chronic hepatitis C virus infection. J Virol 84: 475–481.

Vilasco M, Larrea E, Vitour D, Dabo S, Breiman A, Reqnault B, Riezu JI, Eid P, Prieto J, Meurs EF. 2006. The protein kinase IKKepsilon can inhibit HCV expression independently of IFN and its own expression is downregulated in HCV-infected livers. Hepatology 44:1635–1647.

Wakita T, Taya C, Katsume A, Kato J, Yonekawa H, Kanegae Y, Saito I, Hayashi Y, Koike M, Kohara M. 1998. Efficient conditional transgene expression in hepatitis C virus cDNA transgenic mice mediated by the Cre/loxP system. J Biol Chem 273:9001–9006.

Yoon JC, Shiina M, Ahlenstiel G, Rehermann B. 2008. Natural killer cell function is intact after direct exposure to infectious hepatitis C virions. Hepatology 49:12–21.

JOURNAL OF VIROLOGY, Nov. 2010, p. 11761–11770 Vol. 84, No. 22
0022-538X/10/$12.00 doi:10.1128/JVI.00638-10

Sphingomyelin Activates Hepatitis C Virus RNA Polymerase in a Genotype-Specific Manner▽†

Leiyun Weng,[1] Yuichi Hirata,[2] Masaaki Arai,[3] Michinori Kohara,[2] Takaji Wakita,[4] Koichi Watashi,[4,5] Kunitada Shimotohno,[5,6] Ying He,[7] Jin Zhong,[7] and Tetsuya Toyoda[1]*

Units of Viral Genome Regulation[1] and Viral Hepatitis,[7] Institut Pasteur of Shanghai, Key Laboratory of Molecular Virology and Immunology, Chinese Academy of Sciences, 411 Hefei Road, 200025 Shanghai, People's Republic of China; Department of Microbiology and Cell Biology, Tokyo Metropolitan Institute of Medical Biology, 3-18-22 Honkomagome, Bunkyo-Ku, Tokyo 113-8613, Japan[2]; Pharmacology Laboratory, Pharmacology Department V, Mitsubishi Tanabe Pharma Corporation, 1000 Kamoshida-cho, Aoba-ku, Yokohama 227-0033, Japan[3]; Department of Virology II, National Institute of Health, 1-23-1 Toyama, Shinjuku, Tokyo 132-8640, Japan[4]; Laboratory of Human Tumor Viruses, Department of Viral Oncology, Institute for Virus Research, Kyoto University, Kyoto 606-8507, Japan[5]; and Chiba Institute of Technology, 2-17-1 Tsudamuna, Narashino, Chiba 275-0016, Japan[6]

Received 25 March 2010/Accepted 27 August 2010

Hepatitis C virus (HCV) replication and infection depend on the lipid components of the cell, and replication is inhibited by inhibitors of sphingomyelin biosynthesis. We found that sphingomyelin bound to and activated genotype 1b RNA-dependent RNA polymerase (RdRp) by enhancing its template binding activity. Sphingomyelin also bound to 1a and JFH1 (genotype 2a) RdRps but did not activate them. Sphingomyelin did not bind to or activate J6CF (2a) RdRp. The sphingomyelin binding domain (SBD) of HCV RdRp was mapped to the helix-turn-helix structure (residues 231 to 260), which was essential for sphingomyelin binding and activation. Helix structures (residues 231 to 241 and 247 to 260) are important for RdRp activation, and 238S and 248E are important for maintaining the helix structures for template binding and RdRp activation by sphingomyelin. 241Q in helix 1 and the negatively charged 244D at the apex of the turn are important for sphingomyelin binding. Both amino acids are on the surface of the RdRp molecule. The polarity of the phosphocholine of sphingomyelin is important for HCV RdRp activation. However, phosphocholine did not activate RdRp. Twenty sphingomyelin molecules activated one RdRp molecule. The biochemical effect of sphingomyelin on HCV RdRp activity was virologically confirmed by the HCV replicon system. We also found that the SBD was the lipid raft membrane localization domain of HCV NS5B because JFH1 (2a) replicon cells harboring NS5B with the mutation A242C/S244D moved to the lipid raft while the wild type did not localize there. This agreed with the myriocin sensitivity of the mutant replicon. This sphingomyelin interaction is a target for HCV infection because most HCV RdRps have 241Q.

Hepatitis C virus (HCV) has a positive-stranded RNA genome and belongs to the family *Flaviviridae* (21). HCV chronically infects more than 130 million people worldwide (34), and HCV infection often induces liver cirrhosis and hepatocellular carcinoma (19, 28). To date, pegylated interferon (PEG-IFN) and ribavirin are the standard treatments for HCV infection. However, many patients cannot tolerate their serious side effects. Therefore, the development of new and safer therapeutic methods with better efficacy is urgently needed.

Lipids play important roles in HCV infection and replication. For example, the HCV core associates with lipid droplets and recruits nonstructural proteins and replication complexes to lipid droplet-associated membranes which are involved in the production of infectious virus particles (24). HCV RNA replication depends on viral protein association with raft membranes (2, 30). The association of cholesterol and sphingolipid with HCV particles is also important for virion maturation and infectivity (3). The inhibitors of the sphingolipid biosynthetic pathway, ISP-1 and HPA-12, which specifically inhibit serine palmitoyltransferase (SPT) (23) and ceramide trafficking from the endoplasmic reticulum (ER) to the Golgi apparatus (37), suppress HCV virus production in cell culture but not viral RNA replication by the JFH1 replicon (3). Other serine SPT inhibitors (myriocin and NA255) inhibit genotype 1b replication (4, 29, 33). Very-low-density lipoprotein (VLDL) also interacts with the HCV virion (15).

Sakamoto et al. reported that sphingomyelin bound to HCV RNA-dependent polymerase (RdRp) at the sphingomyelin binding domain (SBD; amino acids 230 to 263 of RdRp) to recruit HCV RdRp on the lipid rafts, where the HCV complex assembles, and that NA255 suppressed HCV replication by releasing HCV RdRp from the lipid rafts (29). In the present study, we analyzed the effect of sphingomyelin on HCV RdRp activity *in vitro* and found that sphingomyelin activated HCV RdRp activity in a genotype-specific manner. We also determined the sphingomyelin activation domain and the activation mechanism. Finally, we confirmed our biochemical data by a HCV replicon system.

* Corresponding author. Mailing address: Unit of Viral Genome Regulation, Institut Pasteur of Shanghai, Chinese Academy of Sciences, 411 Hefei Road, 200025 Shanghai, People's Republic of China. Phone and fax: 86 21 6385 1621. E-mail: ttoyoda@amber.plala.or.jp.

† Supplemental material for this article may be found at http://jvi.asm.org.

▽ Published ahead of print on 15 September 2010.

MATERIALS AND METHODS

HCV RNA polymerase. A C-terminal 21-amino-acid deletion was made to the HCV RdRps of strains HCR6 (genotype 1b) (36), NN (1b) (35), Con1 (1b) (5), JFH1 (2a) (36), J6CF (2a) (25), H77 (1a) (7), and RMT (1a), and the mutants

were purified from bacteria as described previously (36). HCR6 (1b) RdRp with the mutation L245A [RdRp(L245A)] or I253A [RdRp(I253A)] or the double mutation L245A and I253A [RdRp(L245A/I253A)]; JFH1 (2a) RdRp with the mutation(s) A242C/S244D, A242, S244D, or T251Q; J6CF (2a) RdRp with the mutation(s) R241Q, S244D, or R241Q/S244D; and H77 (1a) RdRp(A238S/Q248E) were introduced using an *in vitro* mutagenesis kit (Stratagene) and the oligonucleotides listed in Table S1 in the supplemental material. HCR6 (1b) His_6-tagged RdRp(L245A/I253A) was removed from pET21b/KM (36) and cloned into the BamHI/XhoI site of pGEX-6P-3 (GE), resulting in pGEXHCVHCR6RdRp(L245A/I253A).

***In vitro* HCV transcription.** *In vitro* HCV transcription was performed as described previously (36). Briefly, following 30 min of preincubation without ATP, CTP, or UTP, 100 nM HCV RdRp was incubated in 50 mM Tris-HCl (pH 8.0), 200 mM monopotassium glutamate, 3.5 mM $MnCl_2$, 1 mM dithiothreitol (DTT), 0.5 mM GTP, 50 μM ATP, 50 μM CTP, 5 μM [α-^{32}P]UTP, 200 nM RNA template (SL12-1S), 100 U/ml human placental RNase inhibitor, and the lipid (amount indicated below) at 29°C for 90 min. ^{32}P-labeled RNA products were subjected to 6% polyacrylamide gel electrophoresis (PAGE) containing 8 M urea. The resulting autoradiograph was analyzed with a Typhoon Trio plus image analyzer (GE).

RNA filter binding assay. An RNA filter binding assay was performed as described previously (36). Briefly, 100 nM HCV RdRp and 100 nM ^{32}P-labeled RNA template (SL12-1S) were incubated with or without 0.01 mg/ml egg yolk sphingomyelin in 25 μl of 50 mM Tris-HCl (pH 7.5), 200 mM monopotassium glutamate, 3.5 mM $MnCl_2$, and 1 mM DTT at 29°C for 30 min. After incubation, the solutions were diluted with 0.5 ml of TE (50 mM Tris-HCl [pH 7.5], 1 mM EDTA) buffer and filtered through nitrocellulose membranes (0.45-μm pore size; Millipore). The filter was washed five times with TE buffer, and the bound radioisotope was analyzed by Typhoon Trio plus after being dried.

Enzyme-linked immunosorbent assay (ELISA). Ninety-six-well microtiter plates (Corning) were coated with 250 ng of egg yolk sphingomyelin in ethanol by evaporation at room temperature. After the wells were blocked with phosphate-buffered saline (PBS) and 3% bovine serum albumin (BSA), they were incubated with 1 pmol of the HCV RdRp of HCR6 (1b) wild type (wt) or L245A, I253A, or L245A/I253A mutant; NN (1b); H77 (1a); RMT (1a); J6CF (2a); or JFH1 (2a) wt or A242C/S244D, A242, S244D, or T251Q mutant in Tris-buffered saline (50 mM Tris-HCl [pH 7.5] and 150 mM NaCl) for 1.5 h at room temperature. After being blocked with 3% BSA, the bound HCV RdRp was detected by adding rabbit anti-HCV RdRp serum (1:5,000) (see Fig. S1 in the supplemental material) (17) before incubation with a horseradish peroxidase (HRP)-conjugated anti-rabbit IgG antibody (1:5,000; Southern Biotech). The optical density at 450 nm (OD_{450}) was measured with a Spectra Max 190 spectrophotometer (Molecular Devices) using a TMB (3,3′,5,5′-tetramethylbenzidine) Liquid Substrate System (Sigma).

HCV subgenomic replicon. A D244S mutation was introduced into the HCV strain NN (1b) subgenomic replicon pLMH14 (35), resulting in pLMH(NN)5B(D244S) [where 5B(D244S) is the NS5B protein with the mutation D244S]. The A242C/S244D mutation was introduced into the HCV JFH1 (2a) replicon, pSGR-JFH1/luc (25), resulting in pSGR-JFH1/luc5B(A242C/S244D). The HpaI and XbaI fragment of pSGR-JFH1 (18) was replaced with that of pSGR-JFH1/luc5B(A242C/S244D), resulting in pSGR-JFH15B(A242C/S244D). The A238S/Q248E mutation was introduced into HCV H77 (1a) replicon pHCVrep13(S2204I)/Neo (7) after the neomycin gene was replaced by the firefly luciferase gene [pH77(I)/luc] by insertion of AflII and AscI sites (see Table S1 in the supplemental material), resulting in pH77(I)/luc5B(A238S/Q248E). Subgenomic replicon RNA was transcribed *in vitro* by T7 RNA polymerase using MegaScript (Ambion) after the replicon plasmids were linearized by XbaI (strain NN and JFH1 replicons) or HpaI (strain H77 replicon). Subgenomic replicon RNA was stored at −80°C after being purified by phenol-chloroform extraction and ethanol precipitation.

Replicon assay with myriocin. Huh7.5.1 cells were kindly provided by F. Chisari and were maintained in Dulbecco's modified Eagle's medium (DMEM; Gibco) with 10% fetal bovine serum (FBS; Gibco) (38). HCV replicon RNA (10 μg) was transfected into 4×10^6 Huh7.5.1 cells (1×10^7/ml) in OptiMEM I (Gibco) by electroporation (GenePulser Xcell; Bio-Rad) at 270 V, 100 Ω, and 950 μF. After transfection, the cells were plated in 12-well plates incubated in DMEM–10% FBS. At 6 h after transfection, cells were treated with 0, 5, and 50 nM myriocin. At 4, 54, and 78 h after transfection (48 and 72 h after myriocin treatment), the cells were harvested, and luciferase activity was measured using a Dual-Glo luciferase assay kit and a GloMax 96 Microplate Luminometer (Promega). Luciferase activity was normalized against the activity at 4 h after transfection (26).

HCV JFH1 wt and NS5B(A242C/S244D) replicon cells. Huh7/scr cells were kindly provided by F. Chisari of the Scripps Research Institute and were maintained in Dulbecco's modified Eagle's medium (Gibco) with 10% fetal bovine serum (Gibco). RNA (10 μg each) from SGR-JFH1 and SGR-JFH1 with the mutations A242C/S244D in NS5B [NS5B(A242C/S244D) was transfected into 4×10^6 Huh7/scr cells (1×10^7/ml) in OptiMEM I (GIBCO) by electroporation (GenePulser Xcell; Bio-Rad) at 270 V, 100 Ω, and 950 μF. After transfection, the cells were plated in 10-cm dishes and incubated in DMEM–10% FBS with 1.0 and 0.5 mg/ml G418 (Gibco). JFH1 wt and NS5B(A242C/S244D) replicon cells were maintained in DMEM–10% FBS and 0.5 mg/ml G418.

Membrane floating assay. JFH1 wt and NS5B(A242C/S244D) replicon cells were suspended in two packed cell volumes of hypotonic buffer (10 mM HEPES-NaOH [pH 7.6], 10 mM KCl, 1.5 mM $MgCl_2$, 2 mM DTT, and 1 tablet/25 ml of EDTA-free protease inhibitor cocktail tablets [Roche]) and disrupted by 30 strokes of homogenization in a Dounce homogenizer using a tight-fitting pestle at 4°C. After nuclei were removed by centrifugation at 2,000 rpm for 10 min at 4°C, the supernatant (postnuclear supernatant [PNS]) was treated with 1% Triton X-100 in TNE buffer (25 mM Tris-HCl [pH 7.6] 150 mM NaCl, 1 mM EDTA) for 30 min on ice. The lysates were supplemented with 40% sucrose and centrifuged at 38,000 rpm in a Beckman SW41 Ti rotor (Beckman Coulter) overlaid with 30% and 10% sucrose in TNE buffer at 4°C for 14 h.

Western blotting. Western blotting using anti-HCV RdRp (17), rabbit anti-NS3 (32), anti-NS5A (16) and anti-caveolin-2 was performed as previously published (17).

Reagent. Egg yolk sphingomyelin, cholesterol phosphocholine, myriocin, and rabbit anti-caveolin-2 antibodies were purchased from Sigma. Hexanoyl sphingomyelin, C_6-ceramide, C_8-β-D-glucosyl ceramide, and C_8-β-D-lactosyl ceramide were purchased from Avanti Polar Lipids. [α-^{32}P]UTP was purchased from New England Nuclear.

Statistical analysis. Significant differences were evaluated using *P* values calculated from a Student's *t* test.

Nucleotide sequence accession number. The sequence of HCV RMT has been deposited in the GenBank under accession number AB520610.

RESULTS

Sphingomyelin activation of HCV RNA polymerases of various genotypes. There are several sequence variations in the sphingomyelin binding domain (SBD; amino acids 231 to 260 of HCV RdRp) among HCV genotypes (see Fig. 7A). In order to compare the RdRps of different genotypes of HCV, we purified RdRp from genotypes 1b (strains HCR6, NN, and Con1), 1a (H77 and MRT), and 2a (JFH1 and J6CF) (see Fig. S2 in the supplemental material). First, the effect of ethanol on HCV HCR6 (1b) RdRp transcription was examined because lipids were suspended in ethanol before they were added to the HCV transcription reaction mixture. We found that 2% ethanol did not inhibit HCV transcription (see Fig. S3 in the supplemental material); therefore, all subsequent experiments were performed using less than 2% ethanol.

The kinetics of sphingomyelin activation were analyzed using egg yolk sphingomyelin for HCR6 (1b) RdRp wt (Fig. 1A) and subtype 2a (JFH1 and J6CF) RdRps (Fig. 1B), and *N*-hexanoyl-D-*erythro*-sphingosylphosphorylcholine (hexanoyl sphingomyelin) was used for HCR6 (1b) RdRp wt (Fig. 1C) and subtype 1a (H77 and RMT) RdRps (Fig. 1D). The egg yolk sphingomyelin activation curve of HCR6 (1b) RdRp wt at low concentrations (<0.01 mg/ml) was sigmoid. The transcription activity of HCR6 (1b) RdRp wt increased in a dose-dependent manner. It was activated 11-fold at 0.01 mg/ml and then plateaued (14-fold activation) at 0.1 mg/ml. However, JFH1 (2a) and J6CF (2a) RdRps were activated 2.5-fold and 2.2-fold, respectively, at 0.01 mg/ml sphingomyelin, at which point they plateaued.

Egg yolk sphingomyelin is a mixture. In order to obtain the optimal molar ratio for sphingomyelin activation of HCR6 (1b)

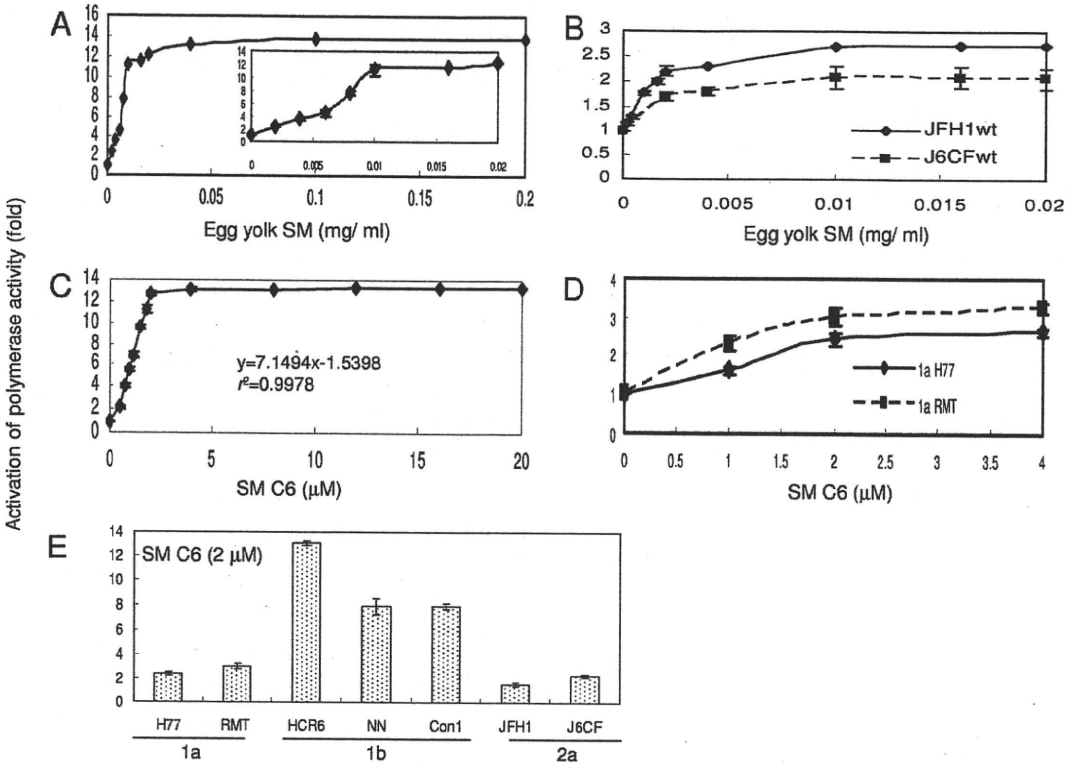

FIG. 1. Sphingomyelin activation of HCV RNA polymerases. (A) Activation kinetics of HCV HCR6 (1b) RdRp wt by egg yolk sphingomyelin (SM). The inset shows activation produced by 0 to 0.02 mg/ml egg yolk sphingomyelin. Activation kinetics of HCV 2a (JFH1 and J6CF) RdRps by egg yolk sphingomyelin (B) and of HCV HCR6 (1b) RdRp wt by hexanoyl sphingomyelin (SM C6) (C). In panel C, the first order of the graph was fitted by linear regression; the calculated equation is indicated in the graph. (D) Activation kinetics of HCV 1a (H77 and RMT) RdRps by hexanoyl sphingomyelin. (E) Activation effect of hexanoyl sphingomyelin on HCV RdRp of various genotypes. HCV RdRp (100 nM) was incubated with or without 2 μM SM C6. The names of the RdRps are indicated below the graph. Mean ± standard deviation of the activation ratio was calculated from three independent experiments.

RdRp wt, its activation kinetics were calculated using hexanoyl sphingomyelin (Fig. 1C, SM C6). The equation for the first-order ratio of hexanoyl sphingomyelin activation according to linear regression fitting was as follows: $y = 7.1494x - 1.5398$, where y is the activation ratio and x is the sphingomyelin concentration ($r^2 = 0.9978$). RdRp activation had almost plateaued at 2 μM hexanoyl sphingomyelin. The activation kinetics of JFH1 (2a) and J6CF (2a) RdRps in egg yolk sphingomyelin were biphasic and plateaued at 0.01 mg/ml. Those of RMT (1a) and H77 (1a) RdRps in hexanoyl sphingomyelin were also biphasic and plateaued at 2 μM. The curve of the first order was fitted by linear regression. The molar ratio of RdRp to hexanoyl sphingomyelin at its plateau was calculated as 1:20.

Because RdRp activation had almost plateaued at 2 μM hexanoyl sphingomyelin, we compared the effect of sphingomyelin on 100 M concentrations of RNA polymerases of the HCV 1a, 1b, and 2a genotypes using 2 μM hexanoyl sphingomyelin (Fig. 1E and Table 1).

Helix-turn-helix structure for sphingomyelin binding and activation. Sphingomyelin binds to the SBD peptide (see HCV SBD in Fig. 7) (29). Initially, we tested whether SBD was the sphingomyelin binding site in HCV RdRp by ELISA (Fig. 2A and Table 1). When the L245 and I253 residues of the SBD peptide were mutated to A, sphingomyelin binding activity was lost (29). We introduced the same mutations in HCV HCR6 (1b) RdRp and purified HCR6 (1b) RdRp with mutations L245A, I253A, and L245A/I253A. Because the C-terminal His-tagged HCR6 RdRp(L245A/I253A) was not soluble, it was solubilized by tagging of glutathione *S*-transferase (GST) sequence at the N terminus but lost polymerase activity. As the L245A/I253A mutant had lost its polymerase activity, polymerase activation was tested only for L245A and I253A (Fig. 2B and Table 1). These results confirmed that SBD located in the finger domain (residues 230E to 263G) successfully achieved sphingomyelin binding in HCV RdRp and that sphingomyelin did not bind to the SBD when the helix-turn-helix structure had been destroyed by the L245A or I253A mutation (29).

The sphingomyelin binding activities of genotype 1a and 2a RdRps were also tested (Fig. 2 and Table 1). Both JFH1 and J6CF were tested for genotype 2a because J6CF (2a) RdRp had an additional amino acid difference at position 241 in the SBD, and its sphingomyelin binding activity was very low (Fig. 2A and 7A; Table 1). J6CF (2a) RdRp(R241Q) showed the same sphingomyelin binding activity as HCR6 (1b) RdRp wt, indicating that 241Q was the critical amino acid for sphingomyelin binding. J6CF (2a) RdRp(S244D) and RdRp(R241Q/S244D) also showed higher sphingomyelin binding activity

TABLE 1. Summary of sphingomyelin activation of HCV RNA polymerase activities

Parameter	Value for the parameter by RdRp genotype, strain, and variant[a]																					
	1b							1a						2a								
	HCR6					NN	Con1	RMT	H77		J6CF				JFH1							
	wt	L245A	I253A	L245A/I253A	D244S	wt	wt	wt	wt	A238S/Q248E	wt	R241Q	S244D	R241Q/S244D	wt	A242C	S244D	A242C/S244D	T251Q
SM binding (%)[b]	100	24.3	30.8	15.5	78.7	93.4	117	144	86.7	82.5	19.3	118	53.1	80.2	70.4	75.5	93.1	92.4	80.7
Activation of polymerase (*n*-fold)[c]	13.0 (11.2)[d]	(2.8)[d]	(2.5)[d]	ND	3.6	7.9	7.9	3.0	2.0	8.1	2.3	4.3	5.6	3.4	1.6	1.0	3.1	4.4	1.8
Activation of RNA binding (*n*-fold)[c]	4.5	2.6	1.7	ND	1.9	ND	ND	ND	1.4	3.3	1.5	3.6	3.2	1.7	1.3	ND	ND	1.4	ND

[a] Numbers were averaged from three independent experiments. ND, not done.
[b] Egg yolk sphingomyelin (SM; 250 ng) was used.
[c] Hexanoyl sphingomyelin (2 μM) was used.
[d] Egg yolk sphingomyelin (0.01 mg/ml) was used.

than the wt ($P < 0.001$) but lower binding than the R241Q mutant. However, S244D showed higher RdRp activation than R241Q ($P < 0.005$), while the RdRp activation ratio of the double mutant (R241Q/S244D) was lower than that of S244D or R241Q, although all of them activated RdRp with sphingomyelin ($P < 0.005$) (Fig. 2A and C and Table 1). For JFH1, when the JFH1 RdRp SBD was modified (A242C/S244D) to allow it to bind with more sphingomyelin than the wt ($P < 0.005$), the mutant JFH1 RdRp(A242C/S244D) was activated more than the wt by sphingomyelin ($P < 0.005$) (Fig. 2A and C; Table 1). The sphingomyelin binding activity of JFH1 RdRp(T251Q) was 80.7% of that of HCR6 (1b), and its activation ratio was 1.8-fold. These results agree that SBD is both the sphingomyelin activation and binding domain and that the domains for these two activities are somehow different.

We determined which amino acid, 242C or 244D, enhanced sphingomyelin binding by comparing HCR6 (1b) and JFH1 (2a) RdRps. Sphingomyelin binding of HCR6 (1b) RdRp(D244S) was 79% of that of the wt ($P < 0.005$) (Fig. 2A and Table 1), and its activation by sphingomyelin was only 3.6-fold (Fig. 2C and Table 1). The sphingomyelin binding of JFH1 (2a) RdRp(A242C) and RdRp(S244D) increased to 75.5% and 93.1%, respectively, of HCR6 (1b) RdRp wt (Fig. 2A and Table 1). This was significantly higher than that of JFH1 (2a) RdRp wt ($P < 0.005$), and the sphingomyelin activation of JFH1 (2a) RdRp(A242C) and RdRp(S244D) was increased 1.0-fold and 3.1-fold, respectively ($P < 0.005$) (Fig. 2C and Table 1). From these mutation analyses of the J6CF and JFH1 RdRps, we concluded that 244D enhanced sphingomyelin binding and RdRp activation.

HCV 1a RdRps were not activated even though sphingomyelin bound to them (Fig. 1E and 2A and Table 1). We then tried to elucidate the domains responsible for sphingomyelin activation. There are 14 amino acids (residues 19, 25, 81, 111, 120, 131, 184, 270, 272, 329, 436, 464, 487, and 540) unique to genotype 1a RdRp in the region of residues 1 to 570 and two amino acid differences unique to 1a RdRp in SBD, i.e., 238A and 248Q (see Fig. 6A). Initially, we focused on the SBD and introduced the A238S and Q248E mutations into the H77 (2a) RdRp SBD (Fig. 2A and D and Table 1). The sphingomyelin binding activity of H77 (2a) RdRp(A238S/Q248E) was similar to that of H77 (2a) RdRp wt. The sphingomyelin activation ratio of H77 (2a) RdRp(A238S/Q248E) was increased 8.1-fold, leading us to conclude that these mutations are essential to sphingomyelin activation.

Effect of lipids on HCV RNA polymerase activity. In order to elucidate the structure of the lipids involved in activation of HCV RdRp, D-lactosyl-β-1,1′-*N*-octanoyl-D-*erythro*-sphingosine [C_8-lactosyl(β) ceramide], D-glucosyl-β1-17-N-octanoyl-D-*erythro*-sphingosine (C_8-β-D-glucosyl ceramide), *N*-hexanol-D-*erythro*-sphingosine (C_6-ceramide), and cholesterol were tested for their abilities to activate RdRp. The relative polymerase activities of 100 nM HCV HCR6 (1b) RdRp activated with 0.01 mg/ml egg yolk sphingomyelin, 2 μM hexanoyl sphingomyelin, 8 μM C_8-lactosyl(β) ceramide, 12 μM C_8-β-D-glucosyl ceramide, 12 μM C_6-ceramide, and 0.02 mg/ml cholesterol were 11.2, 13.0, 5.66, 4.19, 1.12, and 2.25 of that without lipids, respectively (Fig. 3A). The amount of lipids that gave the maximum activation was calculated from the kinetics of the lipids bound to HCR6 (1b) and JFH1 (2a) RdRps (Fig. 3B and

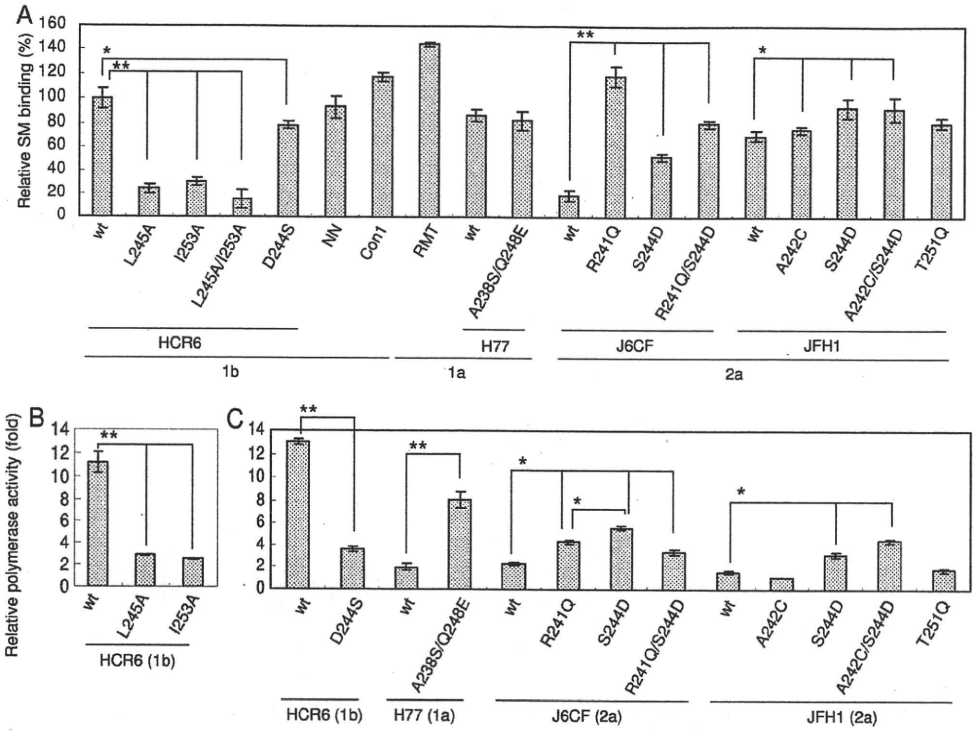

FIG. 2. Sphingomyelin binding and activation of HCV RNA polymerase sphingomyelin binding domain mutants. Names of RdRps are indicated below the graphs. (A) Egg yolk sphingomyelin (SM) binding activity relative to that of HCR6 (1b) RdRp wt. Mean ± standard deviation of the binding was calculated from three independent experiments. (B) Egg yolk sphingomyelin activation of HCR6 (1b) RdRps. RdRps (100 nM) were incubated with or without 0.01 mg/ml egg yolk sphingomyelin. (C) Hexanoyl sphingomyelin activation of the RdRps (RdRp names are indicated below the graphs). HCV RdRps (100 nM) were incubated with or without 2 μM hexanoyl sphingomyelin. The mean ± standard deviation of the activation ratio was calculated from three independent experiments. *, $P < 0.005$; ** $P < 0.001$.

C). C_8-lactosyl(β) ceramide and C_8-β-D-glucosyl ceramide activated HCR6 (1b) RdRp compared with the linear regression kinetics of the reaction with hexanoyl sphingomyelin as it plateaued (Fig. 1C and 3B). Cholesterol activated HCR6 (1b) RdRp slightly but did not activate JFH1 (2a) RdRp (Fig. 3C). We therefore concluded that the phosphocholine of sphingomyelin bound to the SBD of HCV RdRp because the order of HCV RdRp activation was hexanoyl sphingomyelin > C_8-lactosyl(β) ceramide > C_8-β-D-glucosyl ceramide, and C_6-ceramide did not activate HCV HCR6 (1b) RdRp. The polarity of the phosphocholine of sphingomyelin is important for HCV RdRp activation (see Fig. S5 in the supplemental material).

In order to test whether phosphocholine activated HCV RdRp (Fig. 3D), HCR6 (1b) RdRp was incubated with 0.4, 2, 20, 100, and 400 μg and 2, 4, 11, 54, and 100 mg of phosphocholine. Up to 400 μg of phosphocholine did not affect RdRp activity, but more than 2 mg of phosphocholine inhibited RdRp activity.

Effect of sphingomyelin on the template RNA binding of HCV RNA polymerase. The mechanism of HCV RdRp activation was analyzed. RNA polymerase changes its conformation throughout the different transcription steps, and template binding is the first step of transcription (9). Therefore, the effect of sphingomyelin on template RNA binding activity was tested (Fig. 4A and Table 1). Sphingomyelin enhanced the template RNA binding of HCR6 (1b) RdRp wt but not that of JFH1 (2a), H6CF (2a), or H77 (1a) wt RdRp. When the A238S/Q248E mutation was introduced into H77 (1a) RdRp, the RNA binding was enhanced. J6CF (2a) RdRp R241Q and S244D mutants showed similar enhancement of RNA binding, but the R241Q/S244D double mutant did not. The activation effect of RNA binding of HCR6 (1b) RdRp mutants L245A, I253A, and D244S was lower than that of RdRp wt. JFH1 (2a) RdRp wt and RdRp(A242C/S244D) showed similar RNA binding activation levels. Based on a comparison of the sphingomyelin activation of HCR6 (1b) RdRp wt and its mutants which lost sphingomyelin binding with J6CF (2a) RdRp wt and the R241Q and S244D mutants and H77 (1a) RdRp wt and the A238S/Q248E mutant, we concluded that polymerase activation by sphingomyelin was induced mainly via activation of the template RNA binding of RdRp. RNA binding activity of JFH1 (2a) RdRp wt and RdRp(A242C/S244D) was almost saturated because RNA binding of these RdRps was not activated by sphingomyelin (see Fig. S4 in the supplemental material).

HCV RdRp has to be bound with sphingomyelin before or at the same time as it binds to template RNA. After RdRp had bound to the template RNA, sphingomyelin did not enhance template RNA binding strongly (Fig. 4B).

Effect of the sphingomyelin binding domain mutations for HCV replicon activity with myriocin. In order to confirm sphingomyelin activation of HCV polymerase activity in a viral replication system, HCV replicon activity of the loss-of-function mutant HCV NN (1b) NS5B(D244S) and the gain-of-

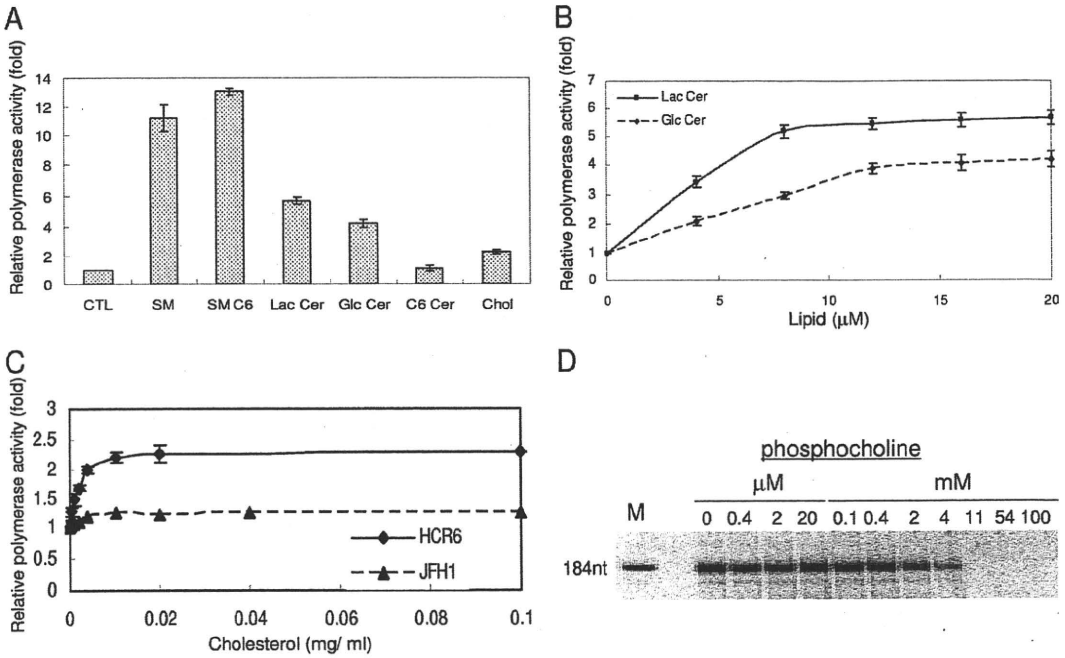

FIG. 3. HCV RNA polymerase activation effect of lipids. (A) Lipid activation of HCR6 (1b) RdRp wt. HCV HCR6 (1b) RdRp wt (100 nM) was incubated with or without (control [CTL]) 0.01 mg/ml egg yolk sphingomyelin (SM), 2 μM hexanoyl sphingomyelin (SM C6), 8 μM C_8-lactosyl(β) ceramide (Lac Cer), 12 μM C_8-β-D-glucosyl ceramide (Glc Cer), 12 μM C_6-ceramide (C6 Cer), or 0.02 mg/ml cholesterol (chol). (B) Activation kinetics of C_8-lactosyl(β) ceramide (Lac Cer) and C_8-β-D-glucosyl ceramide (Glc Cer) on HCR6 (1) RdRp. (C) Activation kinetics of cholesterol on HCR6 (1b) and JFH1 (12a) RdRps. (D) The effect of phosphocholine on HCR6 (1b) RdRp. The mean ± standard deviation of the activation ratio was calculated from three independent experiments.

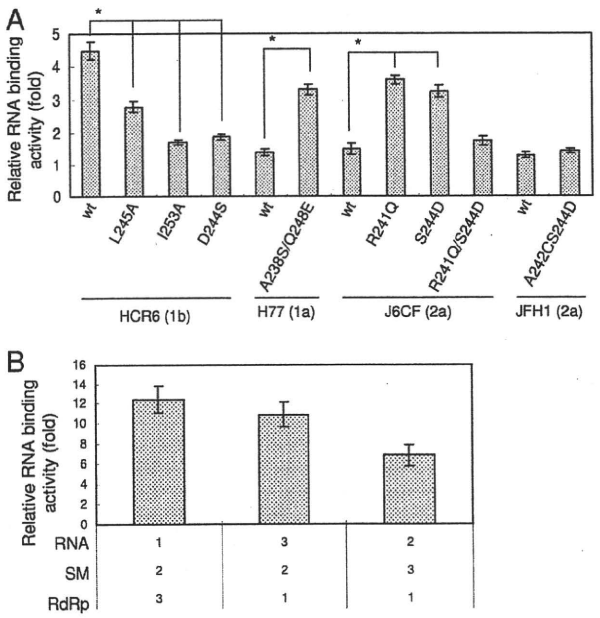

FIG. 4. Sphingomyelin activation of the RNA binding activity of HCV RNA polymerase. (A) Sphingomyelin activation of RNA filter binding of HCV RdRps (RdRp names are indicated below the graph). RdRps and ^{32}P-labeled RNA template (SL12-1S) were incubated with or without egg yolk sphingomyelin (SM), before filtration. (B) Effect of the order of sphingomyelin treatment. Numbers below the graph indicate the order in which the reagents were added. The graph represents the ratio to RNA binding without sphingomyelin. The mean ± standard deviation of the activation ratio was calculated from three independent experiments. *, $P < 0.01$.

function mutants H77 (1a) NS5B(A238S/Q248E) and JFH1 (2a) NS5B(A242C/S244D) were compared with 5 and 50 nM myriocin treatment for 72 h (Fig. 5).

First, HCV replicon activity was compared as the relative luciferase activity (Fig. 5A). Both JFH1 (2a) wt and NS5B(A242C/S244D) replicons showed similar and strong replicon activity ($133 \times 10^3 \pm 12 \times 10^3$ and $138 \times 10^3 \pm 8.5 \times 10^3$, respectively). JFH1 (2a) wt replicon was resistant to myriocin treatment, as reported by Aizaki et al. using other SPT inhibitors (3). The JFH1 (2a) NS5B(A242C/S244D) replicon became sensitive to myriocin but still showed higher replicon activity than NN (1b) or H77 (1a) replicons even at 50 nM myriocin.

To analyze the effect of mutations precisely, the replicon activity relative to each wt strain was compared (Fig. 5B). The JFH1 (2a) wt replicon with 50 nM myriocin showed the same luciferase activity as the wt without myriocin (102% ± 9.6%). JFH1 (2a) NS5B(A242C/S244D) replicon activity was the same as that of the wt without myriocin (103% ± 12%); with 5 nM myriocin it was 84.1% ± 6.6% of the wt level, but with 50 nM myriocin it was 70.3% ± 5.3% of the wt level, which was significantly lower ($P < 0.01$). NN (1b) wt replicon activity was 45.3% ± 6.6% with 5 nM myriocin and 21.7% ± 2.9% with 50 nM myriocin relative to the wt level without myriocin. NN (1b) NS5B(D244S) replicon activity was 72.2% ± 12% without myriocin ($P < 0.05$), 44.0% ± 7.4% with 5 nM myriocin, and 38.1% ± 4.2% with 50 nM myriocin relative to wt level without myriocin, which was significantly higher ($P < 0.01$). Thus, NN (1b) NS5B(D244S) showed lower replicon activity than the wt

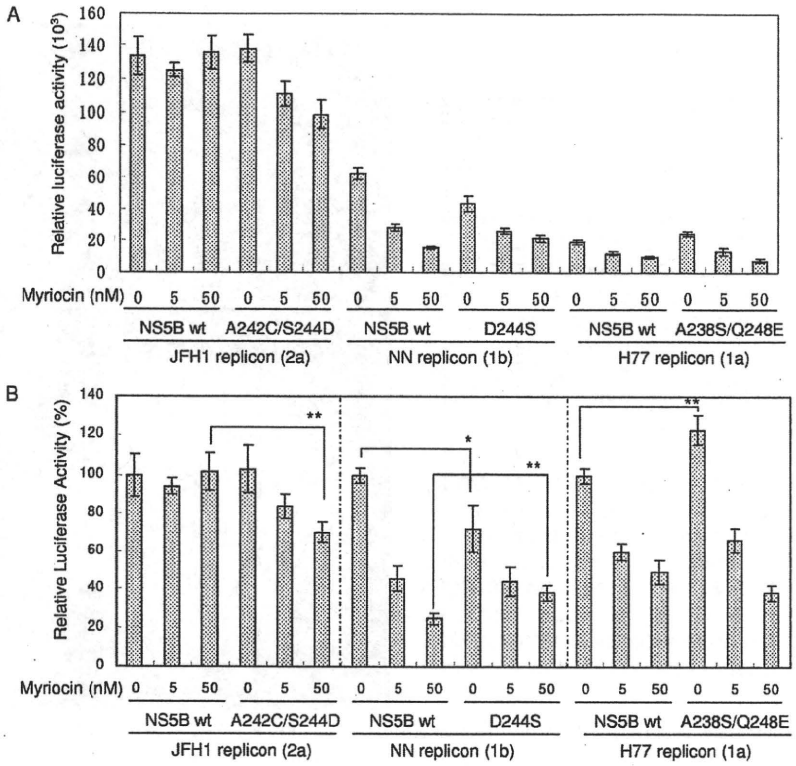

FIG. 5. Myriocin inhibition of HCV replicon activity. Huh7.5.1 cells were incubated with myriocin after transfection with the HCV replicons indicated below the graphs. Means ± standard deviations of the relative luciferase activity at 72 h after myriocin treatment compared to activity at 4 h after transfection (A) and to that of each wt without myriocin (B) were calculated from three independent measurements. *, $P < 0.05$; ** $P < 0.01$.

and was less sensitive to myriocin than the wt. H77 (1a) wt replicon activity was 59.9% ± 4.2% with 5 nM myriocin and 49.2% ± 6.4% with 50 nM myriocin relative to the wt level without myriocin. H77 (1a) NS5B(A238S/Q248E) replicon activity was 123% ± 7.1% without myriocin ($P < 0.01$), 66.1% ± 6.3% with 5 nM myriocin, and 38.0% ± 4.1% with 50 nM myriocin relative to wt level without myriocin. Both H77 (1a) wt and NS5B(A238S/Q248E) replicons were sensitive to myriocin, and the replicon activity of NS5B(A238S/Q248E) was higher than that of the wt.

JFH1 (2a) RdRp(A242C/S244D) localized in the DRM fractions. Myriocin sensitivity of JFH1 (2a) NS5B(A242C/S244D) replicon indicates the importance of 244D in JFH1 NS5B for sphingomyelin binding. To further confirm the role of 244D for recruitment of HCV RdRp to the detergent-resistant membrane (DRM), where the HCV replication complex exists, we compared the distribution of NS5A and NS5B of JFH1 (2a) wt and NS5B(A242C/S244D) in their replicon cells by sucrose density gradient centrifugation of the DRM (Fig. 6). NS5A proteins of both JFH1 (2a) wt and NS5B(A242C/S244D) replicons localized in the DRM fraction where caveolin-2 was present (11, 27), but most of NS5B wt localized in the Triton-soluble fractions. NS5B of JFH1 (2a) NS5B(A242C/S244D) replicon was shifted to the DRM fraction from the soluble fraction. The shift of NS5B(A242C/S244D) localization into the DRM demonstrated that SBD was the DRM localization domain of NS5B and that residue 244D was important for this localization.

DISCUSSION

Hepatitis C virus is an envelope virus, and the lipid components of the virion play important roles in HCV infectivity and virion assembly (3, 15, 20, 24). HCV replication complexes localize in lipid raft structures/DRMs in the membrane frac-

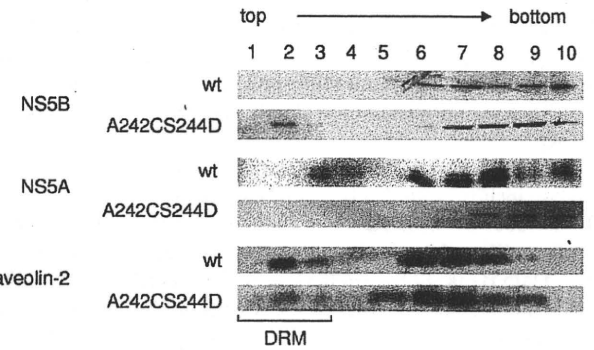

FIG. 6. Membrane floating assay of JFH1 wt and NS5B(A242C/S244D) replicon cells. The PNS fractions of HCV JFH1 (2a) wt and NS5B(A242C/S244D) replicon cells were treated with 1% Triton X-100 in TNE buffer for 30 min at 4°C and subjected to 10 to 40% sucrose gradient centrifugation in TNE buffer. Each fraction was subjected to 10% SDS-PAGE, followed by Western blotting with anti-NS5A, -NS5B, and -caveolin-2 antibodies. Fractions are numbered as indicated at the top of the panel. The DRM fractions (fractions 1 to 3) are indicated.

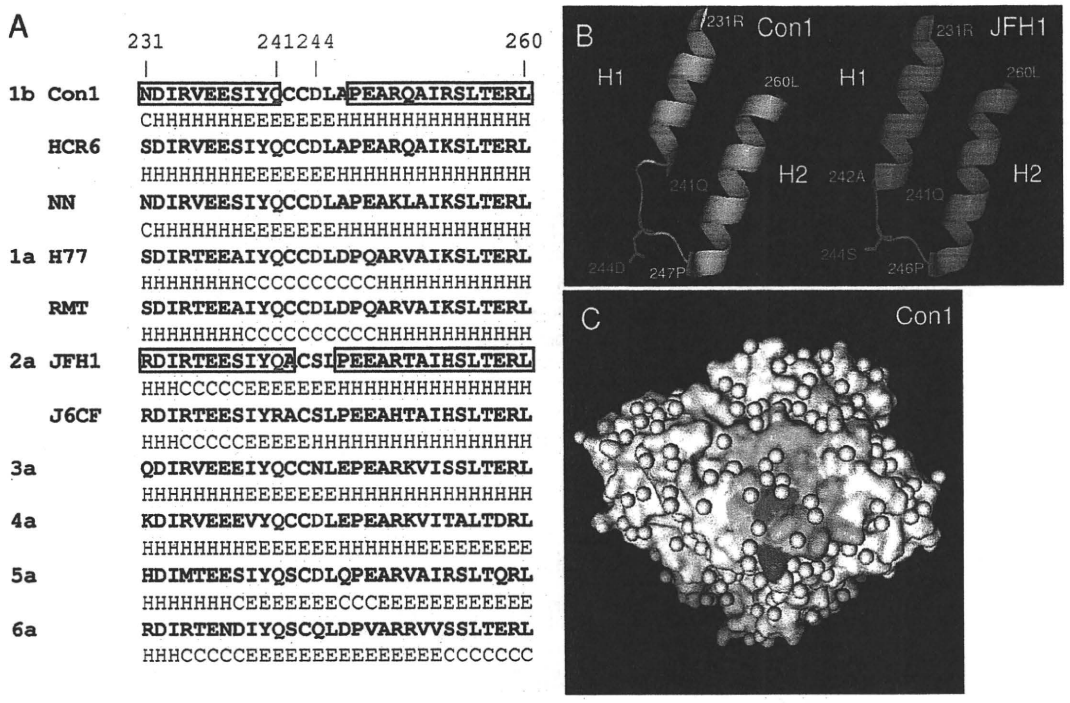

FIG. 7. Sphingomyelin binding domain (SBD) of HCV RNA polymerase. (A) The SBDs (231N to 260L) of HCV RdRps are aligned together with their secondary structure predicted by the Chou-Fasman program (10). The predicted secondary structure is indicated below the sequence as follows: H, α-helix; E, β-sheet; and C, coil. The α-helix structures of HCV Con1 (1b) RdRp and JFH1 (2a) RdRp are boxed in red. Residues 241Q and 244D are indicated in red and green, respectively. The 238A and 248E of the H77 and RMT (1a) RdRps are indicated in purple. GenBank accession numbers of HCV genotypes 3a, 4a, 5a, and 6a are GU814263 (12), GU814265 (12), Y13184 (8), and Y12083 (1), respectively. (B) Comparison of the SBDs of HCV Con1 (1b) (yellow) and JFH1 (2a) RdRps (magenta). The starting and ending amino acids of H1 and H2 are indicated. The sphingomyelin binding site, 241Q, is indicated in red, and 244D of Con1 (1b) and 244S of JFH1 (2a) RdRp are indicated in green. (C) Surface model of HCV Con1 (1b) RdRp. SBD is indicated in yellow, and 241Q and 244D are indicated in red and green, respectively. The structures of the Con1 and JFH1 RdRps were constructed by PyMOL, version 1.1.1 (http://www.pymol.org/). PDB numbers of Con1 (1b) RdRp and JFH1 (2a) RdRp are 3FQL (14) and 3I5K (31), respectively.

tions of subgenomic replicon cells (30). Lipid rafts are composed mainly of sphingomyelin, cholesterol, and glycosphingolipids. Most reports regarding the relationship between lipids and HCV have examined virion assembly, infectivity, and the localization of HCV, but their biochemical interactions have not been reported. Our findings clearly demonstrate that sphingomyelin plays an important role not only in HCV replication complex formation and its localization but also in HCV RdRp activity.

The helix-turn-helix structure of the SBD (residues 230 to 263), which is located between RNA polymerase motifs A and B, has been proposed as the sphingomyelin binding domain of HCV RdRp (29). We compared the SBD of Con1 (1b) (Protein Data Bank [PDB] 3FQL) (14) and JFH1 (2a) (PDB 3I5K) (31) and the secondary structure of the amino acids (201 to 290) in the SBD predicted by the Chou-Fasman program (10) (Fig. 7; see also Fig. S5 in the supplemental material) because the helix structures of the SBD of Con1 (helix 1 [H1], 231N to 241Q; helix 2 [H2], 247A to 260L) and JFH1 (H1, 231R to 242A; H2, 246P to 260L) RdRp fit with those predicted by the Chou-Fasman program. The structures contributing to sphingomyelin binding and activation are H1 and H2 and the junction (turn) between the two helix structures that are similar to the human immunodeficiency virus (HIV) gp120 V3 domain, prion protein (PrP), and β-amyloid peptide (13, 22). Although Con1 (1b) RdRp has a shorter helix structure than JFH1 (2a) RdRp (Fig. 6B), the structures of their SBDs are very similar (Fig. 7; see also Fig. S5). When the helix-turn-helix structure of the SBD was destroyed (HCR6 genotype 1b RdRp mutants L245A and I253A), the RdRp lost sphingomyelin binding activity and lost its activation (Fig. 2).

In order to study the structure-function relationship of the SBD and sphingomyelin, we compared the SBD of genotype 1a, 1b and 2a RdRps and particularly focused on residue 244D in the turn and residues 241Q and 238S/248E in the helix domains. The polar amino acid 241Q and the negatively charged 244D of Con1 (1b) RdRp located on the surface of the RdRp molecule bind and interact with the positively charged choline residue of sphingomyelin (Fig. 7C; see also Fig. S5 in the supplemental material). The positively charged 241R repels the choline residue of sphingomyelin, and as a result, J6CF (a) RdRp wt did not bind to sphingomyelin. J6CF (2a) RdRp(R241Q) showed almost the same sphingomyelin binding activity as HCR6 (1b) RdRp wt. This ionic interaction between SBD and sphingomyelin agrees with the activation of lipids with different sphingosine structures and fatty acid chains (Fig. 3A). JFH1 (2a) RdRp does not interact well with sphingomyelin because it does not have the negatively charged

amino acids at the tip of its turn structure. Once its 244S was changed to D, more sphingomyelin bound to JFH1 (2a) RdRp and activated the RdRp (Fig. 2A and C). The reason for the low activation of J6CF (2a) RdRp(R241Q/S244D) is not clear. Sometimes mutations affect the entire conformation of the molecule. In conclusion, from the comparison of sphingomyelin binding and activation of HCR6 (1b), J6CF (2a), and JFH1 (2a) RdRp SBD mutants, 241Q is the essential amino acid for sphingomyelin binding in the SBD. Amino acid 244D enhanced both binding and RdRp activation.

The *in vitro* sphingomyelin binding and RdRp activation experiments indicate that sphingomyelin binding and its RdRp activation are different biochemical reactions because we found controversial activation rates for sphingomyelin binding and RdRp activation among J6CF (2a) RdRp mutants (Fig. 2). The relationship between sphingomyelin binding and the activation of polymerase activity was studied by comparing genotype 1b and 1a RdRps, both of which bind to sphingomyelin (Fig. 2). However, 1a RdRp is not activated by sphingomyelin because both of the helix structures of 1a RdRp are probably terminated at 238A and 248Q, making its helix structures shorter than those of 1b RdRp (Fig. 6A). The length of the helix structure may be essential for sphingomyelin activation because RdRp changes its structure to bind to template RNA when sphingomyelin binds to SBD (Fig. 4).

HCV RdRp changes its conformations at the early stages of transcription initiation, including the template RNA binding step (6, 9). Sphingomyelin binding is likely to change the conformation of 1b RdRp to recruit template RNA and initiate transcription efficiently. Comparison of the activation ratio of RNA binding and polymerase activity of 1b RdRp, J6CF (2a) RdRp wt and R241Q and S244D mutants, and JFH1 (2a) RdRp wt and mutant A242C/S244D suggests that steps other than RNA binding are also likely to be activated by sphingomyelin.

From a kinetic analysis of sphingomyelin activation (Fig. 1C and D), 20 sphingomyelin molecules are estimated to interact with the SBD of RdRp and activate it because sphingomyelin activation plateaued at 20 sphingomyelin molecules per HCV RdRp molecule. It is not clear whether 20 sphingomyelin molecules form a micelle or a layer structure. However, the structure of sphingomyelin is important for the activation of HCV RdRp because phosphocholine did not activate the RdRp (Fig. 3D).

To confirm these biochemical findings in HCV replication, we tested the effect of SBD mutations in HCV replicon systems with the SPT inhibitor myriocin (Fig. 5) (4, 33) because NA255 was not available. The loss-of-function mutant, HCV NN (1b) NS5B(D244S), showed lower replicon activity than NN (1b) wt and more resistance to 50 nM myriocin, which did not affect the viability of cells (4, 33), than the wt. The gain-of-function mutant, H77 (1a) NS5B(A238S/Q248E), showed higher replicon activity than H77 wt and retained myriocin sensitivity because it had the sphingomyelin binding sites 241Q and 244D. At 50 nM myriocin, another gain-of-function mutant, JFH1 (2a) NS5B(A242C/S244D), was inhibited although its activity was the same as that of JFH1 (2a) wt without myriocin because the JFH1 wt replicon had high replicon activity without myriocin (Fig. 5A). The JFH1 replicon activity may be maximal in the system; therefore, the JFH1 (2a) NS5B(A242C/S244D) replicon did not show higher activity than JFH1 (2a) wt without myriocin while H77 (1a) NS5B(A238S/Q248E) showed higher replicon activity than H77 wt.

The binding and RdRp activation activity of the amino acid 244 mutants by sphingomyelin did not differ greatly from the wt *in vitro*. However, the myriocin sensitivity of JFH1 (2a) NS5B(S244D) was demonstrated clearly. That of H77 (1a) NS5B(A238S/Q248E) indicated that sphingomyelin binding was the target of myriocin inhibition, not the sphingomyelin activation of RdRp. These data confirm the importance of 241Q, 244D, and the helix structure in SBD for HCV replication in the cells.

Sphingomyelin is the major component of the lipid raft structure/DRM where the HCV genome replicates. To confirm that the SBD is the membrane binding site of HCV RdRp, we analyzed the localization of NS5B of JFH1 (2a) wt and NS5B(A242C/S244D) replicons by membrane floating assay (Fig. 6). JFH1 (2a) NS5B wt did not localize in the DRM. However, the localization of NS5B of the JFH1 (2a) NS5B(A242C/S244D) replicon shifted to the DRM from the soluble fractions. Previously, HCV NS5B was believed to localize in the DRM by its C-terminal hydrophobic sequences (21). However, our data demonstrate that the SBD is the membrane localization domain of HCV NS5B, which agrees with the myriocin sensitivity of JFH1 (2a) NS5B(A242C/S244D) replicons (Fig. 5) and the release of HCV 1b NS5B from the DRM by another SPT inhibitor, NA255 (29).

This is the first report of RNA polymerase activation by lipids. Twenty sphingomyelin molecules interact with SBD, particularly with residues 241Q and 244D of HCV (1b) RdRp, and change the conformation of the RdRp in order to recruit RNA templates. At the same time, HCV RdRp molecules may be aligned on the sphingomyelin layer formed via interactions between the hydrocarbon chains of sphingosine and fatty acids via placement of their SBD into the layer (Fig. 7C). Consistent with previous research (3, 23, 37), our findings explain why the inhibitors of the sphingolipid biosynthetic pathway influence subgenomic replicons derived from HCV genotypes 1a and 1b but not those derived from JFH1 (2a) (Fig. 5). Most HCV isolates have 241Q in NS5B, and some of them also have 244D (Fig. 7A). These sphingomyelin interactions are new targets for the treatment of HCV.

ACKNOWLEDGMENTS

We thank C. Rice and R. Bartenshlager for the HCV H77 and Con1 plasmids, respectively. We also thank F. Chisari for Huh7.5.1 and Huh7/src cells.

This work was supported by a grant-in-aid from the Chinese Academy of Sciences (O514P51131 and KSCX1-YW-10), the Chinese 973 project (2009CB522504), and the Chinese National Science and Technology Major Project (2008ZX10002-014).

REFERENCES

1. **Adams, N. J., R. W. Chamberlain, L. A. Taylor, F. Davidson, C. K. Lin, R. M. Elliott, and P. Simmonds.** 1997. Complete coding sequence of hepatitis C virus genotype 6a. Biochem. Biophys. Res. Commun. **234**:393–396.
2. **Aizaki, H., K. J. Lee, V. M. Sung, H. Ishiko, and M. M. Lai.** 2004. Characterization of the hepatitis C virus RNA replication complex associated with lipid rafts. Virology **324**:450–461.
3. **Aizaki, H., K. Morikawa, M. Fukasawa, H. Hara, Y. Inoue, H. Tani, K. Saito, M. Nishijima, K. Hanada, Y. Matsuura, M. M. Lai, T. Miyamura, T. Wakita, and T. Suzuki.** 2008. Critical role of virion-associated cholesterol and sphingolipid in hepatitis C virus infection. J. Virol. **82**:5715–5724.
4. **Amemiya, F., S. Maekawa, Y. Itakura, A. Kanayama, A. Matsui, S. Takano, T. Yamaguchi, J. Itakura, T. Kitamura, T. Inoue, M. Sakamoto, K. Yamau-**

chi, S. Okada, A. Yamashita, N. Sakamoto, M. Itoh, and N. Enomoto. 2008. Targeting lipid metabolism in the treatment of hepatitis C virus infection. J. Infect. Dis. **197**:361–370.
5. **Binder, M., D. Quinkert, O. Bochkarova, R. Klein, N. Kezmic, R. Bartenschlager, and V. Lohmann.** 2007. Identification of determinants involved in initiation of hepatitis C virus RNA synthesis by using intergenotypic replicase chimeras. J. Virol. **81**:5270–5283.
6. **Biswal, B. K., M. M. Cherney, M. Wang, L. Chan, C. G. Yannopoulos, D. Bilimoria, O. Nicolas, J. Bedard, and M. N. James.** 2005. Crystal structures of the RNA-dependent RNA polymerase genotype 2a of hepatitis C virus reveal two conformations and suggest mechanisms of inhibition by non-nucleoside inhibitors. J. Biol. Chem. **280**:18202–18210.
7. **Blight, K. J., J. A. McKeating, J. Marcotrigiano, and C. M. Rice.** 2003. Efficient replication of hepatitis C virus genotype 1a RNAs in cell culture. J. Virol. **77**:3181–3190.
8. **Chamberlain, R. W., N. J. Adams, L. A. Taylor, P. Simmonds, and R. M. Elliott.** 1997. The complete coding sequence of hepatitis C virus genotype 5a, the predominant genotype in South Africa. Biochem. Biophys. Res. Commun. **236**:44–49.
9. **Chinnaswamy, S., I. Yarbrough, S. Palaninathan, C. T. Kumar, V. Vijayaraghavan, B. Demeler, S. M. Lemon, J. C. Sacchettini, and C. C. Kao.** 2008. A locking mechanism regulates RNA synthesis and host protein interaction by the hepatitis C virus polymerase. J. Biol. Chem. **283**:20535–20546.
10. **Chou, P. Y., and G. D. Fasman.** 1974. Prediction of protein conformation. Biochemistry **13**:222–245.
11. **Fujimoto, T., H. Kogo, K. Ishiguro, K. Tauchi, and R. Nomura.** 2001. Caveolin-2 is targeted to lipid droplets, a new "membrane domain" in the cell. J. Cell Biol. **152**:1079–1085.
12. **Gottwein, J. M., T. K. Scheel, B. Callendret, Y. P. Li, H. B. Eccleston, R. E. Engle, S. Govindarajan, W. Satterfield, R. H. Purcell, C. M. Walker, and J. Bukh.** Novel infectious cDNA clones of hepatitis C virus genotype 3a (strain S52) and 4a (strain ED43): genetic analyses and *in vivo* pathogenesis studies. J. Virol. **84**:5277–5293.
13. **Hammache, D., G. Pieroni, N. Yahi, O. Delezay, N. Koch, H. Lafont, C. Tamalet, and J. Fantini.** 1998. Specific interaction of HIV-1 and HIV-2 surface envelope glycoproteins with monolayers of galactosylceramide and ganglioside GM3. J. Biol. Chem. **273**:7967–7971.
14. **Hang, J. Q., Y. Yang, S. F. Harris, V. Leveque, H. J. Whittington, S. Rajyaguru, G. Ao-Ieong, M. F. McCown, A. Wong, A. M. Giannetti, S. Le Pogam, F. Talamas, N. Cammack, I. Najera, and K. Klumpp.** 2009. Slow binding inhibition and mechanism of resistance of non-nucleoside polymerase inhibitors of hepatitis C virus. J. Biol. Chem. **284**:15517–15529.
15. **Huang, H., F. Sun, D. M. Owen, W. Li, Y. Chen, M. Gale, Jr., and J. Ye.** 2007. Hepatitis C virus production by human hepatocytes dependent on assembly and secretion of very low-density lipoproteins. Proc. Natl. Acad. Sci. U. S. A. **104**:5848–5853.
16. **Ishii, N., K. Watashi, T. Hishiki, K. Goto, D. Inoue, M. Hijikata, T. Wakita, N. Kato, and K. Shimotohno.** 2006. Diverse effects of cyclosporine on hepatitis C virus strain replication. J. Virol. **80**:4510–4520.
17. **Kashiwagi, T., K. Hara, M. Kohara, K. Kohara, J. Iwahashi, N. Hamada, H. Yoshino, and T. Toyoda.** 2002. Kinetic analysis of C-terminally truncated RNA-dependent RNA polymerase of hepatitis C virus. Biochem. Biophys. Res. Commun. **290**:1188–1194.
18. **Kato, T., T. Date, M. Miyamoto, A. Furusaka, K. Tokushige, M. Mizokami, and T. Wakita.** 2003. Efficient replication of the genotype 2a hepatitis C virus subgenomic replicon. Gastroenterology **125**:1808–1817.
19. **Kiyosawa, K., T. Sodeyama, E. Tanaka, Y. Gibo, K. Yoshizawa, Y. Nakano, S. Furuta, Y. Akahane, K. Nishioka, R. H. Purcell, et al.** 1990. Interrelationship of blood transfusion, non-A, non-B hepatitis and hepatocellular carcinoma: analysis by detection of antibody to hepatitis C virus. Hepatology **12**:671–675.
20. **Lambot, M., S. Fretier, A. Op De Beeck, B. Quatannens, S. Lestavel, V. Clavey, and J. Dubuisson.** 2002. Reconstitution of hepatitis C virus envelope glycoproteins into liposomes as a surrogate model to study virus attachment. J. Biol. Chem. **277**:20625–20630.
21. **Lemon, S., C. Walker, M. Alter, and M. Yi.** 2007. Hepatitis C virus, p. 1253–1304. *In* D. M. Knipe, P. M. Howley, D. E. Griffin, R. A. Lamb, M. A. Martin, B. Roizman, and S. E. Straus (ed.), Fields virology, 5th ed. Lippincott Williams & Wilkins, Philadelphia, PA.
22. **Mahfoud, R., N. Garmy, M. Maresca, N. Yahi, A. Puigserver, and J. Fantini.** 2002. Identification of a common sphingolipid-binding domain in Alzheimer, prion, and HIV-1 proteins. J. Biol. Chem. **277**:11292–11296.
23. **Miyake, Y., Y. Kozutsumi, S. Nakamura, T. Fujita, and T. Kawasaki.** 1995. Serine palmitoyltransferase is the primary target of a sphingosine-like immunosuppressant, ISP-1/myriocin. Biochem. Biophys. Res. Commun. **211**: 396–403.
24. **Miyanari, Y., K. Atsuzawa, N. Usuda, K. Watashi, T. Hishiki, M. Zayas, R. Bartenschlager, T. Wakita, M. Hijikata, and K. Shimotohno.** 2007. The lipid droplet is an important organelle for hepatitis C virus production. Nat. Cell Biol. **9**:1089–1097.
25. **Murayama, A., T. Date, K. Morikawa, D. Akazawa, M. Miyamoto, M. Kaga, K. Ishii, T. Suzuki, T. Kato, M. Mizokami, and T. Wakita.** 2007. The NS3 helicase and NS5B-to-3'X regions are important for efficient hepatitis C virus strain JFH-1 replication in Huh7 cells. J. Virol. **81**:8030–8040.
26. **Murayama, A., L. Weng, T. Date, D. Akazawa, X. Tian, T. Suzuki, T. Kato, Y. Tanaka, M. Mizokami, T. Wakita, and T. Toyoda.** 2010. RNA polymerase activity and specific RNA structure are required for efficient HCV replication in cultured cells. PLoS Pathog. **6**:e1000885.
27. **Ostermeyer, A. G., J. M. Paci, Y. Zeng, D. M. Lublin, S. Munro, and D. A. Brown.** 2001. Accumulation of caveolin in the endoplasmic reticulum redirects the protein to lipid storage droplets. J. Cell Biol. **152**:1071–1078.
28. **Saito, I., T. Miyamura, A. Ohbayashi, H. Harada, T. Katayama, S. Kikuchi, Y. Watanabe, S. Koi, M. Onji, Y. Ohta, et al.** 1990. Hepatitis C virus infection is associated with the development of hepatocellular carcinoma. Proc. Natl. Acad. Sci. U. S. A. **87**:6547–6549.
29. **Sakamoto, H., K. Okamoto, M. Aoki, H. Kato, A. Katsume, A. Ohta, T. Tsukuda, N. Shimma, Y. Aoki, M. Arisawa, M. Kohara, and M. Sudoh.** 2005. Host sphingolipid biosynthesis as a target for hepatitis C virus therapy. Nat. Chem. Biol. **1**:333–337.
30. **Shi, S. T., K. J. Lee, H. Aizaki, S. B. Hwang, and M. M. Lai.** 2003. Hepatitis C virus RNA replication occurs on a detergent-resistant membrane that cofractionates with caveolin-2. J. Virol. **77**:4160–4168.
31. **Simister, P., M. Schmitt, M. Geitmann, O. Wicht, U. H. Danielson, R. Klein, S. Bressanelli, and V. Lohmann.** 2009. Structural and functional analysis of hepatitis C virus strain JFH1 polymerase. J. Virol. **83**:11926–11939.
32. **Tsukiyama-Kohara, K., S. Tone, I. Maruyama, K. Inoue, A. Katsume, H. Nuriya, H. Ohmori, J. Ohkawa, K. Taira, Y. Hoshikawa, F. Shibasaki, M. Reth, Y. Minatogawa, and M. Kohara.** 2004. Activation of the CKI-CDK-Rb-E2F pathway in full genome hepatitis C virus-expressing cells. J. Biol. Chem. **279**:14531–14541.
33. **Umehara, T., M. Sudoh, F. Yasui, C. Matsuda, Y. Hayashi, K. Chayama, and M. Kohara.** 2006. Serine palmitoyltransferase inhibitor suppresses HCV replication in a mouse model. Biochem. Biophys. Res. Commun. **346**:67–73.
34. **Wasley, A., and M. J. Alter.** 2000. Epidemiology of hepatitis C: geographic differences and temporal trends. Semin. Liver Dis. **20**:1–16.
35. **Watashi, K., N. Ishii, M. Hijikata, D. Inoue, T. Murata, Y. Miyanari, and K. Shimotohno.** 2005. Cyclophilin B is a functional regulator of hepatitis C virus RNA polymerase. Mol. Cell **19**:111–122.
36. **Weng, L., J. Du, J. Zhou, J. Ding, T. Wakita, M. Kohara, and T. Toyoda.** 2009. Modification of hepatitis C virus 1b RNA polymerase to make a highly active JFH1-type polymerase by mutation of the thumb domain. Arch. Virol. **154**:765–773.
37. **Yasuda, S., H. Kitagawa, M. Ueno, H. Ishitani, M. Fukasawa, M. Nishijima, S. Kobayashi, and K. Hanada.** 2001. A novel inhibitor of ceramide trafficking from the endoplasmic reticulum to the site of sphingomyelin synthesis. J. Biol. Chem. **276**:43994–44002.
38. **Zhong, J., P. Gastaminza, G. Cheng, S. Kapadia, T. Kato, D. R. Burton, S. F. Wieland, S. L. Uprichard, T. Wakita, and F. V. Chisari.** 2005. Robust hepatitis C virus infection in vitro. Proc. Natl. Acad. Sci. U. S. A. **102**:9294–9299.

DOI 10.1002/eji.200940203 Eur. J. Immunol. 2010. 40: 940–948

Frontline

European Journal of Immunology

DEAD/H BOX 3 (DDX3) helicase binds the RIG-I adaptor IPS-1 to up-regulate IFN-β-inducing potential

Hiroyuki Oshiumi, Keisuke Sakai, Misako Matsumoto and Tsukasa Seya

Department of Microbiology and Immunology, Hokkaido University Graduate School of Medicine, Kita-ku, Sapporo, Japan

Retinoic acid-inducible gene-I (RIG-I)-like receptors (RLR) are members of the DEAD box helicases, and recognize viral RNA in the cytoplasm, leading to IFN-β induction through the adaptor IFN-β promoter stimulator-1 (IPS-1) (also known as Cardif, mitochondrial antiviral signaling protein or virus-induced signaling adaptor). Since uninfected cells usually harbor a trace of RIG-I, other RNA-binding proteins may participate in assembling viral RNA into the IPS-1 pathway during the initial response to infection. We searched for proteins coupling with human IPS-1 by yeast two-hybrid and identified another DEAD (Asp-Glu-Ala-Asp) box helicase, DDX3 (DEAD/H BOX 3). DDX3 can bind viral RNA to join it in the IPS-1 complex. Unlike RIG-I, DDX3 was constitutively expressed in cells, and some fraction of DDX3 is colocalized with IPS-1 around mitochondria. The 622-662 a.a DDX3 C-terminal region (DDX3-C) directly bound to the IPS-1 CARD-like domain, and the whole DDX3 protein also associated with RLR. By reporter assay, DDX3 helped IPS-1 up-regulate IFN-β promoter activation and knockdown of DDX3 by siRNA resulted in reduced IFN-β induction. This activity was conserved on the DDX3-C fragment. DDX3 only marginally enhanced IFN-β promoter activation induced by transfected TANK-binding kinase 1 (TBK1) or I-kappa-B kinase-ε (IKKε). Forced expression of DDX3 augmented virus-mediated IFN-β induction and host cell protection against virus infection. Hence, DDX3 is an antiviral IPS-1 enhancer.

Key words: DDX3 · IFN-β · IPS-1 · RIG-I-like receptors · Viral infection

See accompanying Commentary by Mulhern and Bowie

Introduction

Retinoic acid-inducible gene-I (RIG-I) and melanoma differentiation-associated gene 5 (MDA5) are cytoplasmic RNA helicases [1–3], which signal the presence of viral RNA through the adaptor, IFN-β promoter stimulator-1 (IPS-1) (also known as mitochondrial antiviral signaling protein/caspase recruitment domain (CARD) adaptor inducing IFN-β (Cardif)/virus-induced signaling adaptor) to produce IFN-β [4–7]. IPS-1 localizes on the outer membrane of the mitochondria *via* its C-terminus [6]. Its N-terminus consists of a CARD domain, which interacts with the CARD domains of RIG-I and MDA5. Viral RNA resulting from penetration or replication are believed to assemble in the CARD-interacting helicase complex to activate the cytoplasmic IFN-inducing pathway. Although non-infected cells usually express minimal amounts of RIG-I/MDA5, the final output of type I IFN is efficiently induced at an early stage of infection to protect host cells from viral spreading.

Once IPS-1 is activated, the kinase complex consisting of TANK-homologous proteins and virus-activated kinases induce nuclear translocation of IFN regulatory factor-3 (IRF-3) to activate the IFN promoter [8]. NAK-associated protein 1, TANK-binding kinase 1 (TBK1) and I-kappa-B kinase-ε (IKKε) are components of the kinase complex that phosphorylates IRF-3 to induce type I IFN [9, 10]. RIG-I recognizes products of various RNA viruses, while MDA5 recognizes products of picornaviruses

Correspondence: Dr. Tsukasa Seya
e-mail: seya-tu@pop.med.hokudai.ac.jp

[1, 11]. RIG-I and MDA5 share the helicase domain, which is classified into the DEAD (Asp-Glu-Ala-Asp) box helicase family, and the domain can bind to various RNA structures. 5′-triphosphate RNA or short dsRNA is a ligand of RIG-I, whereas long dsRNA is a ligand of MDA5 [1, 12]. However, these RIG-I-like receptors (RLR) are usually up-regulated to a sufficient level secondary to IFN stimulation, suggesting that other molecular mechanisms are responsible for the initial sensing of viral RNA.

Here, we looked for molecules that bind IPS-1 by yeast two-hybrid, and found a DEAD box helicase, DDX3 (DEAD/H BOX 3), as a component of the complex of IPS-1. DDX3 facilitated IPS-1-mediated IFN-β induction to confer high antiviral potential on early infection phase of host cells. This is the first report showing that DDX3 is an IPS-1 complement factor for antiviral IFN-β induction in host infectious cells.

Results

Involvement of DDX3 in the IPS-1 complex

IPS-1 is constitutively present on the mitochondrial membrane and plays a central role in the cytoplasmic IFN-inducing pathway. We searched for proteins that bind IPS-1 in yeast. Using bait plasmids with the IPS-1 CARD region (aa 6–136), we screened a human lung cDNA library to isolate IPS-1 CARD-interacting proteins. We identified one clone, #62 that encodes the DDX3 C-terminal region (aa 276–662), which included partial DEAD box and helicase superfamily C-terminal regions (Fig. 1A). Their interaction was confirmed in HEK293FT cells by immunoprecipitation (IP), where DDX3 and IPS-1 were coupled (Fig. 1B). We confirmed that the C-terminal fragments of DDX3, at least 622-662 a.a, bound IPS-1 (data not shown). Taken together with the results of the yeast two-hybrid assay, the C-terminal portions of DDX3 directly bind the CARD-like region of IPS-1.

RIG-I and MDA5 helicases also bind the IPS-1 CARD domain [4]. In general, RNA helicases make a large molecular complex, and sometimes form homo- or hetero-oligomers. RIG-I binds to LGP2 helicase, and forms homo-oligomers during Sendai virus infection [11]. Hence, we examined whether DDX3 was associated with the RLR proteins by i.p. RIG-I and MDA5 co-precipitated with DDX3 (Fig. 2A), suggesting that DDX3 is involved in the complex of IPS-1 that interacts with RIG-I and/or MDA5. DDX3 bound the C-terminal helicase domain including the RD region of RIG-I (Fig. 2B). Thus, additional interaction may occur between DDX3 and RIG-I/MDA5. IPS-1 localizes to the membrane of mitochondria [6]. Three-color imaging analysis indicated that DDX3 in part co-localized to the IPS-1-mitochodria complex in non-stimulated resting HeLa cells, which express undetectable amounts of RLR (Fig. 2C and data not shown). These results together with accumulating evidence infer that non-infected cells harbor the complex of DDX3 and IPS-1 with minimal amounts of RIG-I/MDA5.

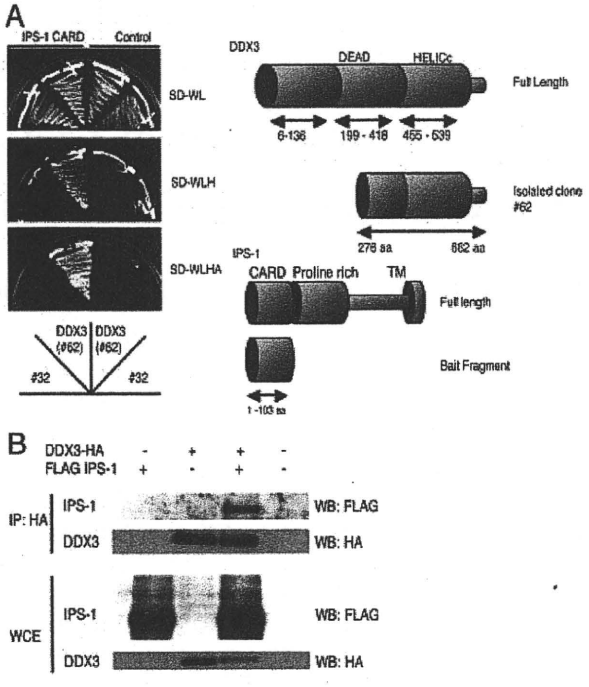

Figure 1. DDX3 binds IPS-1. (A) DDX3 partial cDNA fragment (aa 276–662) isolated by the yeast two-hybrid screening interacted with the IPS-1 CARD region (aa 1–103) in yeast. Tryptophan- and leucine-depleted synthetic dextrose medium plate (SD-WL) is non-selective, and tryptophan-, leucine- and histidine-depleted synthetic dextrose medium plate (SD-WLH) and tryptophan-, leucine-, histidine- and alanine-depleted synthetic dextrose medium (SD-WLHA) plates are selective plates. Empty bait plasmid (pGBKT7) was used for a negative control. (B) FLAG-tagged IPS-1 and HA-tagged DDX3 expression vectors were transiently transfected into HEK293FT cells by FuGeneHD reagent. 24 h after transfection, cell lysates were prepared, and IP was carried out using anti-HA Ab. The immunoprecipitates were analyzed by western blot using anti-HA or FLAG Ab. Data are representative of three independent experiments.

DDX3 promotes IPS-1-mediated IFN-β promoter activation

Forced expression of IPS-1 causes the activation of transcription from the IFN-β promoter. To ascertain the role of DDX3 in IFN-β production, we carried out reporter gene analysis to see the enhancing effect of DDX3 on IPS-1-mediated IFN-β promoter activation. Overexpression of DDX3 alone caused little activation of the promoter; however, the promoter activation was more augmented by minimal addition of DDX3 to IPS-1 than by overexpressed IPS-1 alone (Fig. 3A). This suggested that DDX3 enhanced IPS-1-mediated signaling despite the lack of RIG-I overexpression. To establish which region of DDX3 is important for IFN-β enhancer activity, partial DDX3 fragments were overexpressed with IPS-1, and IFN-β promoter activation was examined. The N-terminal region (aa 1–224, aa 224–487, aa 488–621) barely enhanced promoter activation (data not shown), but the C-terminal region (622–662) activated the promoter (Fig. 3B). These data indicated that the C-terminal region of DDX3 is important for the binding to IPS-1 and potentiation of the IPS-1 pathway.

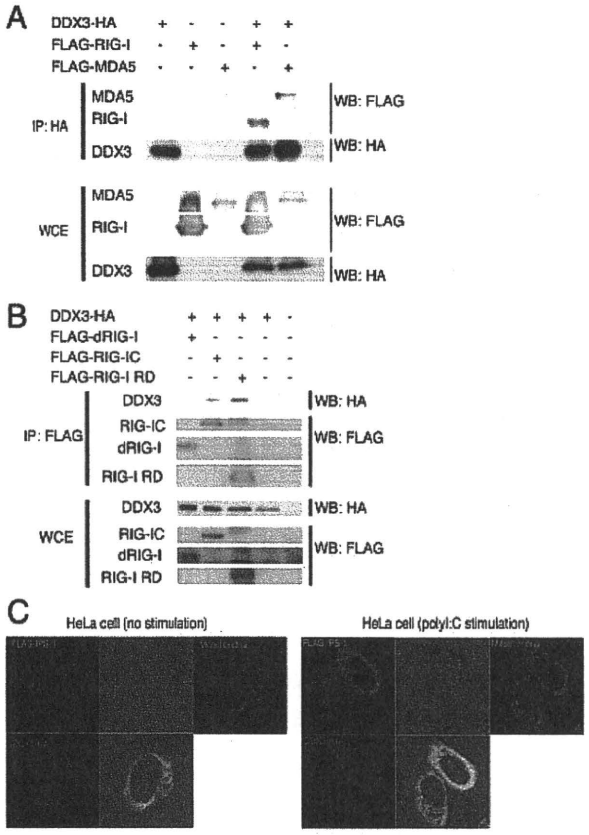

Figure 2. DDX3 joins the complex of RIG-I, MDA5 and IPS-1. (A) RIG-I and MDA5 co-precipitate with DDX3. HA-tagged DDX3 was expressed in HEK293FT cells, together with FLAG-tagged MDA5 or RIG-I, and 24 h after transfection, IP was performed using anti-HA Ab and analyzed by western blotting. (B) The C-terminal region of RIG-I participates in complex formation with DDX3. FLAG-tagged RIG-I fragments and HA-tagged DDX3 were expressed in HEK293 cells, and 24 h after transfection, IP was performed using anti-HA Ab and analyzed by western blotting. (C) DDX3 colocalizes with IPS-1. Flag-tagged IPS-1 and HA-tagged DDX3 were transfected into HeLa cells together with or without polyI:C. After 24 h, cells were fixed with formaldehyde and stained with anti-HA polyclonal and anti-FLAG monoclonal Ab. Alexa488 (DDX3-HA) or Alexa633 Ab was used for second Ab. Mitochondria was stained with Mitotracker Red. DDX-3 partially colocalized with IPS-1. Data are representative of three independent experiments.

DDX3 as a component of initial RNA sensor

RIG-I and MDA5 are IFN-inducible proteins, only traces of which exist in an early phase (<2 h) in the cytoplasm where viral RNA replicate. Previous reports showed that DDX3 binds RNA of poly rA or duplexed RNA [13, 14], and our protein analysis solidified this issue: DDX3 efficiently bound polyI:C and stem-loop RNA of viral origin in a solution (data not shown). DDX3 as well as IPS-1 were expressed even without any stimulation (Fig. 2C and 4A and B) and bound each other in the cytoplasm (Fig. 2C). Hence, DDX3 is a cytoplasmic molecule that can detect viral RNA produced in infected cells.

Knockdown studies suggested that polyI:C-mediated IFN promoter activation was abrogated in DDX3-deficient cells even in the presence of overexpressed RIG-I or MDA5 (Fig. 5). DDX3 silencing happened with two different siRNA. Thus, DDX3 may enable RIG-I and IPS-1 to confer activation of the cytoplasmic RNA-sensing pathway on virus-infected cells.

The IFN-β-inducing pathway involves IRF-3 kinases TBK1 and IKKε, which may be targets of DDX3 [15, 16]. By *in vitro* reporter analysis, increasing amounts of DDX3 barely affected IFN-β promoter activation by TBK1 and IKKε (Fig. 6A and B). Slight TBK1-enhancing activity could manage to be detected with DDX3 when decreasing amounts of TBK1 was used in the assay (Fig. 6C and D).

HeLa cells induced the mRNA of RIG-I and IFN-β in response to polyI:C stimulation within 1 h (Fig. 4A). More exactly, IFN-β induction was ~30 min faster than RIG-I induction in response to polyI:C. IFN-β mRNA induction was peaked around 3 h post stimulation, while RIG-I induction continued to increase >3 h (Fig. 4A). When HEK293 cells were infected with vesicular stomatitis virus (VSV) (a RIG-I-stimulating virus), the IFN-β mRNA was induced from 6 h, and by that time no RIG-I message was generated (Fig. 4B–D). The RIG-I message began to appear >8 h and was markedly increased (Fig. 4B and D). In either case, no up-regulation was observed with DDX3 but sufficiently present in the cytoplasm (Fig. 4C). Furthermore, overexpression of DDX3 in HeLa cells resulted in potential prevention of VSV propagation (Fig. 7). However, the distribution profiles of DDX3 and IPS-1 were barely altered in response to polyI:C stimulation (Fig. 2C). The results allow us to interpret that when viral RNA enter the cytoplasm of infected cells, the RNA first induce a small amount of IFN-β in conjunction with the complex containing trace RIG-I and then the induced IFN-β fosters intensive RIG-I/MDA5 induction. The complex is reconstituted together with upcoming RIG-I/MDA5 to amplify the cytoplasmic IFN-inducing pathway. Although the molecular reconstitution was not visible with overexpressed proteins by confocal analysis, DDX3 may act as an enhancing factor for initial RNA-sensing by the IPS-1 complex and conducts the rapid response to viral RNA to facilitate the IPS-1 signaling.

Discussion

We identified DDX3 as a protein that bound to the IPS-1 CARD region, duplexed RNA and RLR. Although the DDX3 helicase domain is a DEAD box type similar to those of RIG-I and MDA5, DDX3 does not have a signaling domain corresponding to the CARD domain. Therefore, DDX3 may not act as a signal sensor of RNA viruses, as RIG-I and MDA5 do. Considering the role of DDX3 in host RNA metabolism, it is more likely that DDX3 acts as a scaffold for RIG-I (even under the presence of low copy numbers of RIG-I) and intensifies IPS-1 signaling similar to LGP2 [11, 17]. RNA molecules usually form a complex with various

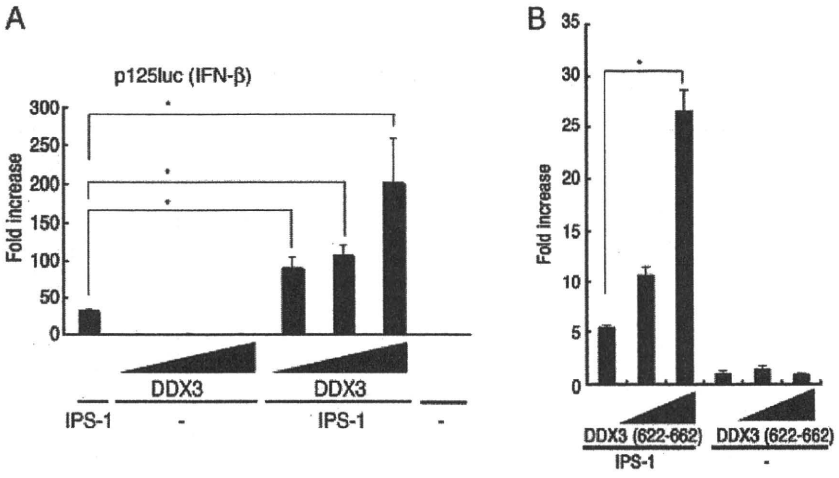

Figure 3. The C-terminal region of DDX3 participates in enhancing IPS-1-mediated IFN-β promoter activation. (A) Activation of IFN-β promoter was examined by reporter gene assay. HEK293 cells were transfected with DDX3- (100, 200 or 300 ng) and/or IPS-1 (100 ng)-encoding plasmids, together with reporter (p125luc) and control plasmids (Renilla luciferase) into 24-well plates. (B) The plasmids for expression of DDX3 (622-662 aa) and IPS-1 or the former only were transfected into HEK293 cells in 24-well plates together with p125luc reporter plasmid. After 24 h, the activation of reporter was measured. Data show mean fold induction+SD of three independent assays. $*p<0.05$, Student's t-test.

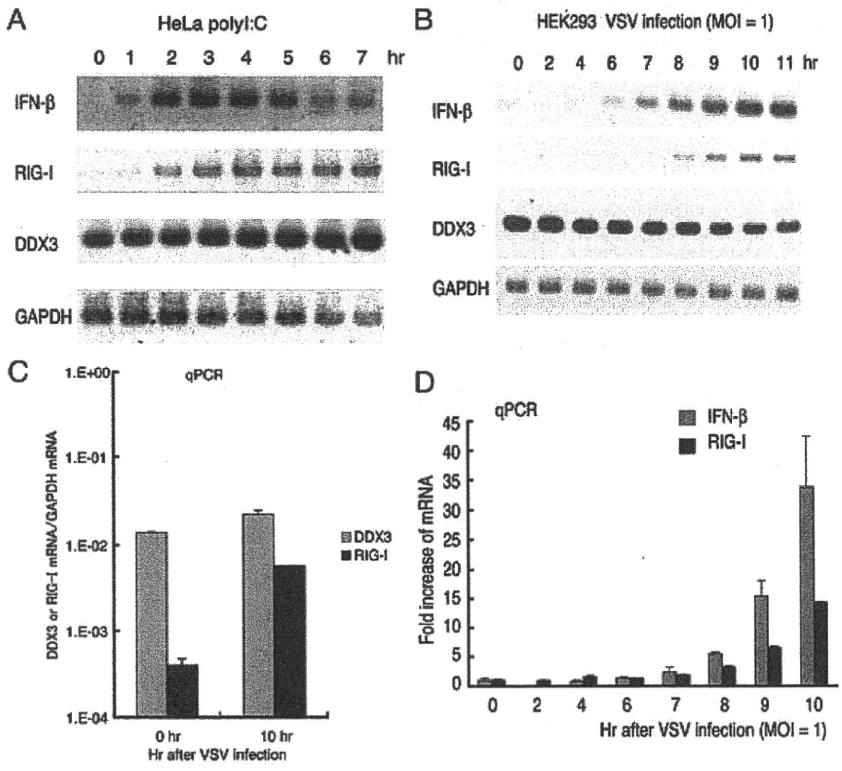

Figure 4. Earlier induction of IFN- than RIG-I in virus-infected cells. (A) Early induction of IFN-β in response to polyI:C. HeLa cells were stimulated with 50 μg/mL of polyI:C for indicated hours. Total RNA was extracted with TRIZOL and RT-PCR was carried out to examine the kinetics of expressions of DDX3, IFN-β, RIG-I and GAPDH (control). (B) IFN-β mRNA induction by VSV infection. HEK293 cell were infected with VSV at MOI = 1, and then total RNA was extracted with TRIZOL reagents at indicated times. The reverse transcription with random primers and PCR at 33 cycle were performed to detect RIG-I, DDX3 or IFN-β expression. Data are representative of three independent experiments. (C) Marked induction of RIG-I in VSV-infected cells. HEK293 cells were infected with VSV at MOI = 1, and then the total RNA was extracted with TRIZOL reagent at indicated times. The relative amounts of RIG-I or DDX3 mRNA were quantified by RT-qPCR, in which the mRNA of GAPDH was used for endogenous internal control. (D) Fold increase of IFN-β or RIG-I mRNA by VSV infection. The amount of IFN-β or RIG-I cDNA was determined by quantitative PCR. The fold increases were calculated by dividing the values of each time point by that of 0 h sample of IFN-β or RIG-I. Data show mean+SD pooled from three independent experiments.

proteins, such as 5′-end capping enzymes or translation initiation factors. Viral RNA also tends to couple with host proteins to replicate and translate RNA. DDX3 capturing RNA may function either in the molecular complex of RIG-I/MDA5/IPS-1 or in the complex of the translation machinery.

Recently, DDX3 was reported to up-regulate IFN-β induction by interacting with IKKε in the kinase complex [18]. IKKε is an NF-κB-inducible gene, whereas the DDX3-IPS-1 complex is constitutively present prior to infection. DDX3 may bind IKKε after IKKε is generated secondary to NF-κB activation [15]. Another report suggested that DDX3 interacts with TBK1 to synergistically stimulate the IFN-β promoter [16]. The report further suggested that DDX3 is recruited to the IFN promoter and acts like a transcription factor [16]. These reports also show that not C-terminal but N-terminal region of DDX3 is required for enhancing the IKKε- or TBK1-mediated IFN promoter activation. We showed that unlike these previous reports, the C-terminal region of DDX3 is important for the IPS-1 activation. These observations indicate that DDX3 is involved in RIG-I signaling at multiple steps. The involvement of DDX3 at several steps is not surprising, because DDX3 plays several roles in RNA metabolisms, such as RNA translocation or mRNA translation.

In cytoplasm, there are large amounts of DDX3 and only trace amounts of RIG-I in resting cells. Therefore, when the virus initially infects human cells, the viral RNA would encounter DDX3 before RIG-I capture the viral RNA. We demonstrated that the initial IPS-1 complex for RNA-sensing involves DDX3 in addition to trace RIG-I to cope with the early phase of infection. This IPS-1 complex activates downstream signal by involving a minute amount of viral RNA. What happens in actual viral infection is to first induce IFN-β and then RIG-I (Fig. 4B), suggesting that the initial IFN-β mRNA arises independent of the virus-induced RIG-I. Once IFN-β and RIG-I mRNA are up-regulated by viral RNA, the IPS-1 complex turns constitutionally different: the complex contains high amounts of RIG-I, which may directly capture viral RNA without DDX3. Our results indicate that the early IPS-1 complex formed in the early stages of virus-infected cells induce minute IFN-β with a mode different from the conventional IPS-1 pathway that RIG-I solely capture viral RNA and activates IPS-1. By retracting DDX3 from the complex by siRNA, only a minimal IFN-β response emerges merely with preexisting RIG-I and IPS-1, suggesting DDX3 to be a critical signal enhancer in the early IPS-1 complex. Development of a method to chase endogenous DDX3 will be required to test our interpretation.

The RIG-I generation occurring > 8 h post RNA virus challenge makes the complex direct the conventional IFN-inducing pathway harboring sufficient RIG-I/MDA5. Previous reports [13, 14] and our RNA-binding analysis also speculated that one of the RNA-capture proteins is DDX3 since DDX3 tightly binds polyI:C and dsRNA in fluid phase. These RNA-capture proteins may have a role in the IPS-1-involving molecular platform in cells with early virus infection when only a trace RIG-I protein is expressed. This interpretation fits the result that DDX3 acts predominantly on an early phase of virus infection (Fig. 4B and 7).

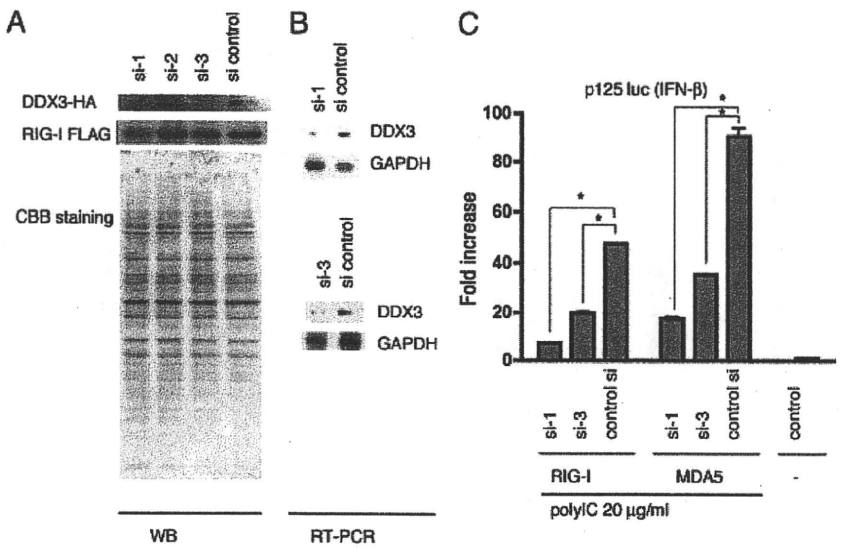

Figure 5. Knockdown of DDX3. (A) Negative control or DDX3 targeting siRNA (20 pmol), DDX3 si-1, -2 or -3, were transfected into HEK293 cells in 24-well plates, together with HA-tagged DDX3 or FLAG-tagged RIG-I expression plasmids, and after 48 h, cell lysates were prepared and analyzed by western blotting with anti-HA or anti-FLAG Ab, and the same membrane was stained with CBB. (B) DDX3 si-1, -3 or control siRNA was transfected into HEK293 cells, and after 48 h, expression of endogenous DDX3 mRNA was examined by RT-PCR. (C) DDX3 si-1, -3 or control siRNA was transfected into HEK293 cells with reporter plasmids and RIG-I- or MDA5 expression plasmid (100 ng). Forty-eight hours after transfection, cells were stimulated with polyI:C (20 μg/mL) with dextran for 4 h, and activation of the reporter was measured. siRNA for DDX3 reduced RIG-I- or MDA5-mediated p125luc activation. Data are representative of three independent experiments (A,B). Data show mean fold increase+SD pooled from three independent experiments (C). *$p<0.05$, Student's t-test.

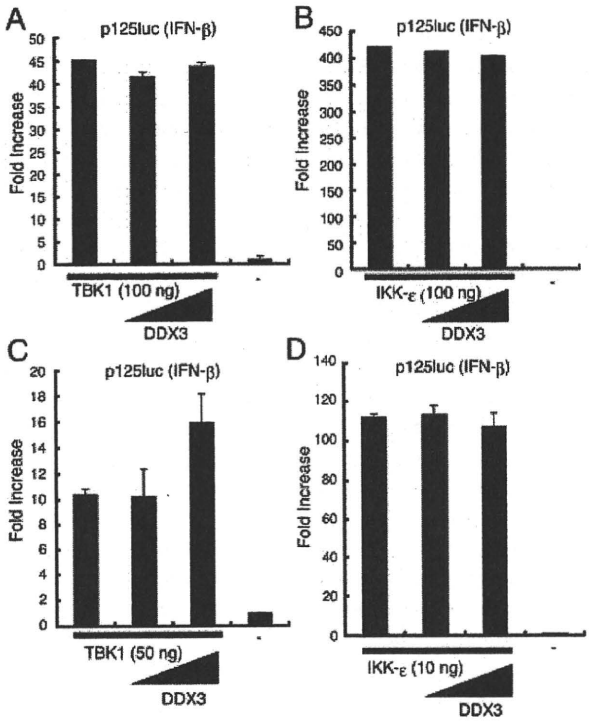

Figure 6. TBK1 and IKKε are not main targets for DDX3-mediated IFN-β up-regulation. (A–D) The activation of IFN-β promoter was examined by reporter gene assay. HEK293 cells were transfected in 24-well plates with DDX3 (0, 100 or 300 ng)-, TBK1 (0, 50 or 100 ng)- or IKKε (0, 10 or 100 ng)-encoding plasmid together with reporter (p125luc) and control plasmid. After 24 h, the cell lysate was prepared and the luciferase activities were measured. Data show mean+SD of three independent experiments.

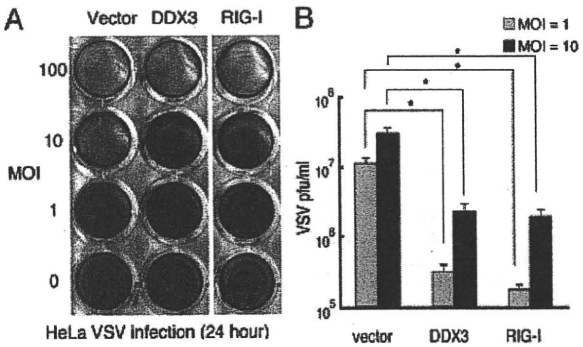

Figure 7. VSV infection is suppressed by overexpressed DDX3. (A) HeLa cells were transfected with DDX3, RIG-I or empty vector. After 24 h, the transfected cells were infected with VSV at indicated MOI. 24 h after VSV infection, the cells were fixed with formaldehyde and stained with crystal violet. (B) The VSV titers of culture supernatant of HeLa cells infected with VSV at MOI = 1 or 10 were measured by plaque assay. Data show mean+SD of three independent experiments. *$p<0.05$, Student's t-test.

Proteins involved in type I IFN induction are found ubiquitinated for their functional regulation. It has been reported that TRIM25 [19] and Riplet/RNF135 [20] act as ubiquitin ligases to activate RIG-I for IFN-β induction in their different sites of RIG-I ubiquitination. Another ubiquitin ligase RNF125 polyubiquitinates RIG-I through Lys48, leading to degradation of RIG-I [21]. The RIG-I level is highly susceptible to not only IFN but also ubiquitination in host cells. In addition, many viral factors may suppress the RIG-I function. It remains unknown what factor maintains a minimal level of RIG-I/MDA5 in resting cells. We favor the interpretation that DDX3 can be an alternative factor for compensating the low RLR contents in a certain infectious situation such that RIG-I is degraded or poorly up-regulated by other viral factors.

DDX3 is functionally complicated since its protective role against viruses may be modulated after the synthesis of viral proteins. DDX3 couples with the HCV core protein in HCV-infected cells and promotes viral replication [22]. This alternative function of DDX3 is accelerated by the HCV core protein, since the core protein withdraws DDX3 from the IFN-β-inducing facility, leading to suppression of IFN-β induction and positive regulation of HCV propagation in infected cells. DDX3 is also involved in HIV RNA translocation [14]. The DDX3 gene is conserved among eukaryotes, and Ded1 is a budding yeast homolog [23]. Ded1 helicase is essential for initiation of host mRNA translation, and human DDX3 can complement the lethality of Ded1-null yeast cells [24, 25]. Hence, another function of DDX3 is to bind viral RNA to modulate RNA replication and translocation. It is not surprising that DDX3 is implicated in various steps of RNA metabolism in cells with both host and viral RNA.

Materials and methods

Cell culture and reagents

HEK293 cells and HEK293FT cells were maintained in Dulbecco's Modified Eagle's low or high glucose medium (Invitrogen, Carlsbad, CA, USA) supplemented with 10% heat-inactivated FBS (Invitrogen) and antibiotics. HeLa cells were maintained in MEM (Nissui, Tokyo, Japan) supplemented with 10% heat-inactivated FBS. Anti-FLAG M2 mAb, anti-HA polyclonal Ab, were purchased from Sigma-Aldrich (St. Louis, MO, USA). Alexa Fluor®-conjugated secondary Ab were from Invitrogen.

Plasmids

DDX3 cDNA encoding the entire ORF was cloned into pCR-blunt vector using primers, DDX3N F-Xh (CTC GAG CCA CCA TGA GTC ATG TGG CAG TGG AA) and DDX3C R-Ba (GGA TCC GTT ACC CCA CCA GTC AAC CCC) from human lung cDNA library. To make an expression plasmid, HA tag was fused at the C-terminal end of the full length DDX3 (pEF-BOS DDX3-HA). pEF-BOS DDX3 (1–224 aa) vector was made by using primers DDX3 N-F-Xh and DDX3D1 (GGA TCC GGC ACA AGC CAT CAA GTC TCT TTT C).